River Scour Monitoring System for Pipeline Threat Prevention

Contract Number: 693JK31810011



Prepared For:
US DOT PHMSA

Prepared By:
Samuel T. Ariaratnam, Ph.D., P.E.
Arizona State University
ariaratnam@asu.edu

Tyler Lich, P.Eng.
Xylem/Pure Technologies HM
tyler.lich@xylem.com

SEPTEMBER 2021

TABLE OF CONTENTS

1.0 Introduction/Project Background 8

2.0 Review of Existing Threat Prevention Measures 11

3.0 River Scour Monitoring Systems (RSS) 12

- 3.1 Introduction 12
- 3.2 Installation 14

4.0 Site Installations 14

- 4.1 Introduction 14
- 4.2 Tongue River Crossing, North Dakota 14
- 4.3 Elk River Crossing, Kansas 17
- 4.4 Freeman River Crossing, Alberta 21

5.0 Field Data Collection 24

- 5.1 Tongue River Crossing, North Dakota 24
- 5.2 Elk River Crossing, Kansas 25
- 5.3 Freeman River Crossing, Alberta 28

6.0 Software and Hardware 30

- 6.1 Software/Website Upgrade 30
- 6.2 River Scour Monitoring System Hardware Upgrade 34

7.0 Vortex-Induced Vibrations (VIV) 41

- 7.1 VIV Background 41
- 7.2 Phase change of multiphase flow 43
- 7.3 Vortex-induced vibration analysis 49
- 7.4 Comparison of bending stress of exposed pipe caused by fluid force 54
- 7.5 VIV conclusions 62

8.0 Conclusions and Recommendations 64

9.0 References 66

APPENDIX A – Samples of Daily Data Collection

LIST OF FIGURES

Figure 1. Configuration of River Scour Monitoring Systems 12

Figure 2. Prototype River Scour Detection System at Kinder Morgan Site 13

Figure 3. Exposure (due to river scour) of Pipeline at Kinder Morgan Demo Site 13

Figure 4. Tongue River Crossing 14

Figure 5. Sensor Installation at Tongue River 15

Figure 6. Tongue River Site Overview 15

Figure 7. Tongue River Scour System Above Ground Equipment 16

Figure 8. Elk River Crossing 17

Figure 9. Elk River Crossing Sensor Installation 18

Figure 10. Elk River Above Ground Equipment 18

Figure 11. Elk River Upstream Sensor 1 Overview 19

Figure 12. Elk River Upstream Sensor 2 Site Over 20

Figure 13. Elk River Downstream Sensor 1 Site Overview 20

Figure 14. Elk River Downstream Sensor 2 Site Overview 21

Figure 15. Freeman River Crossing in March 2020 22

Figure 16. Sensor Installations at the Freeman River from Left to Right: Upstream 1, Upstream 2 and Downstream 1 22

Figure 17. Above Ground River Scour Monitoring Systems at the Freeman River from Left to Right: Upstream 1, Upstream 2 and Downstream 1 23

Figure 18. Pipeline Temperatures on Tongue River Pipeline #1 24

Figure 19. Pipeline Temperatures on Tongue River Pipeline #2 25

Figure 20. Pipeline Temperatures on Elk River Pipeline #1 26

Figure 21. Pipeline Temperatures on Elk River Pipeline #1 26

Figure 22. Elk River Crossing Bathymetry 27

Figure 23. Elk River Crossing Plan and Profile 27

Figure 24. Pipeline Temperatures on Freeman River Pipeline 28

Figure 25. Pipeline Right-of-Way on the Freeman River Pipeline 28

Figure 26. Freeman River Pipeline Crossing from the Installed Camera System (May 2020) 29
Figure 27. Survey Boat Containing High-Resolution Multi-Beam Sonar 29
Figure 28. Software Operating Diagram (Version 1.0) 30
Figure 29. Input Screen for RSS Monitoring (Version 2.0) 31
Figure 30. Custom Sensor Calibration (Version 2.0) 31
Figure 31. Pure Hub Display Software Upgrade (Version 2.0) 32
Figure 32. Correlation with SCADA Pressure Data (Version 3.0) 33
Figure 33. Auto Bias Adjustment and Scour Detection Threshold (Version 3.0) 33
Figure 34. Incorporation of Jupyter Notebook Source (Version 4.0) 34
Figure 35. Schematic Drawings of Version 1.0 RSS Units 35
Figure 36. Incorporation of Jupyter Notebook Source (Version 4.0) 36
Figure 37. Pipe Sensor Installation Details 36
Figure 38. Version 3.0 Mechanical Configuration Upgrades 37
Figure 39. Version 3.0 Electrical Configuration Upgrades 38
Figure 40. Version 3.0 Pole Mounted Installation 38
Figure 41. Version 3.0 Non-Intrusive Base Added to Pole 39
Figure 42. Version 4.0 RSS Camera Addition 39
Figure 43. Version 5.0 RSS Unit with Enhanced Security Measures 40
Figure 44. Velocity Distribution with Pipe Exposed 50% 42
Figure 45. Velocity Distribution with Pipe Exposed 75% 42
Figure 46. Velocity Distribution with Pipe Exposed 100% 42
Figure 47. Phase Changes of the Riverbed at Different Moments of Fluid Flow at M1 47
Figure 48. Phase Changes of the Riverbed at Different Moments of Fluid Flow at M2 47
Figure 49. Phase Changes of the Riverbed at Different Moments of Fluid Flow at M3 47
Figure 50. Phase Changes of the Riverbed at Different Moments of Fluid Flow at M4 48
Figure 51. Phase Changes of the Riverbed at Different Moments of Fluid Flow at M5 48
Figure 52. Phase Changes of the Riverbed at Different Moments of Fluid Flow at M6 48
Figure 53. Phase Changes of the Riverbed at Different Moments of Fluid Flow at M7 49
Figure 54. Phase Changes of the Riverbed at Different Moments of Fluid Flow at M8 49

Figure 55. Phase Changes of the Riverbed at Different Moments of Fluid Flow at M9 …………… 49

Figure 56. Fluid Force at X Direction (Drag) and Y Direction (Lift) of M1, M2 and M3 ……………… 51

Figure 57. Fluid Force at X Direction (Drag) and Y Direction (Lift) of M4, M5 and M6 ……………… 52

Figure 58. Fluid Force at X Direction (Drag) and Y Direction (Lift) of M7, M8 and M9.……………… 53

Figure 59. Subsea Pipeline with "Free-span" …………………………………………………………………… 54

Figure 60. Maximum Bending Normal Stress, Maximum Displacement, and Maximum Shear Stress of the Free Span Pipeline at a) Different Fluid Velocity and b) Different Pipe Exposure Rates with *l* = 36 m …… 56

Figure 61. a) Maximum Bending Normal Stress, b) Maximum Shear and c) Maximum Displacement of the Free Span Pipeline at Y Direction with Rates with *l* = 36 m and *l* = 18 m ……………………… 59

Figure 62. a) Maximum Bending Normal Stress, b) Maximum Shear and c) Maximum Displacement of the Free Span Pipeline at X Direction with Rates with *l* = 36 m and *l* = 18 m ……………………… 60

LIST OF TABLES

Table 1. Failure of Hazardous Liquid Pipelines from Depletion of Cover at Inland Bodies of Water 1993 to 2011 (adapted from PHMSA, 2013)…………………………………………………. 9

Table 2. Tongue River Installation Locations - Line 2 …………………………………………………….. 16

Table 3. Tongue River Installation Locations - Line 13 ……………………………………………………. 16

Table 4. Elk River Sensor Installation Locations - Pipeline 1 ……………………………………………… 19

Table 5. Elk River Sensor Installation Locations - Pipeline 2 ……………………………………………… 19

Table 6. Model Number and Conditions ……………………………………………………………………… 43

Table 7. Maximum Bending Normal Stress, Maximum Displacement and Maximum Shear Stress of the Free Span Pipeline with *l* = 36 m ……………………………………………………………… 58

Table 8. Maximum Bending Normal Stress, Maximum Displacement and Maximum Shear Stress of the Free Span Pipeline with *l* = 36 m and *l* = 36 m ……………………………………………… 61

ABSTRACT

Hazardous liquid pipelines are mandated to maintain a minimum cover depth below the river bottom at crossings of inland bodies of water with widths greater than 100 feet (30 meters) from high water mark to high water mark as per 49 CFR Part 195.248, Subpart D – Construction. These prescribed burial depths apply during the initial pipeline construction phase and not during system operation. Over time, river scour results in a reduction in the prescribed depth of cover that can compromise the pipelines. The objective of this research is the development of a "River Scour Monitoring System (RSS)" to benefit society by serving as an "active" monitoring system capable of determining the degree of scour in a riverbed thereby alerting pipeline operators should the amount of cover of the pipeline become reduced. The proposed technology is based on a temperature gradient decay method for monitoring a subject pipeline river crossing for scour conditions. Field demonstrations at crossing sites will provide a validation of the applicability for detecting depletion of cover above an installed pipeline. The Arizona State University-Xylem/PureHM Inc. team brings complementary expertise to the project. This report presents the development, and field validation testing of five River Scour Monitoring Systems installed at three different water crossings.

1.0 INTRODUCTION/PROJECT BACKGROUND

The objective of this research is the development of a “River Scour Monitoring System” to benefit society by serving as an “active” monitoring system capable of determining the degree of scour in a riverbed thereby alerting pipeline operators should the amount of cover of the pipeline become reduced. This conforms to the objectives of 49 CFR 195.452, which addresses pipeline integrity management in “high consequence” areas such as river crossings.

The pipeline infrastructure and volume of products transported have continued to grow as demand for energy has increased. At the same time, the pipeline infrastructure system has continued to age. Over the next two decades, the demand for energy is projected to reach record levels. This increased demand for energy combined with the expansion of cities and suburban areas will require the aging pipeline infrastructure not only to expand but to deliver energy services reliably and safely in support of the nation’s economy. Although the U.S. has a well-developed system for protecting the public and environment from dangers of hazardous liquid and natural gas pipeline failures, there is always the chance that a pipeline can leak leading to catastrophe. Pipeline leaks can be “dangerous” to people, to the natural environment, to public land, and private property.

Hazardous liquid pipelines are mandated to maintain a minimum cover depth of 48 inches (1219 mm) below the river bottom at crossings of inland bodies of water with widths greater than 100 feet (30 meters) from high water mark to high water mark (49 CFR Part 195.248, Subpart D – Construction). The exception is when solid rock requiring blasting is encountered where the minimum burial depth is relaxed to 18 inches (457 mm). An issue is that these prescribed burial depths apply during the initial pipeline construction phase and not during system operation. Over time, river scour results in a reduction in the prescribed depth of cover. Subsequently, accurate and reliable scour and leak detection systems are critical for minimizing volume of spills.

49 CFR Part 195.452 requires that hazardous pipeline operators develop and implement an integrity management program to protect pipelines, especially those that could affect high-consequence areas in the event of a failure. Included in this requirement is the need for operators to perform a “critical, investigative, risk-based evaluation of their leak detection capabilities.” Integrity Management for river crossings requires the use of “effective” leak detection capabilities. Unfortunately, the ability of commonly used leak detection systems such as Computational Pipeline Monitoring (CPM) to identify and report low-level leaks in hazardous liquid pipelines, especially in high consequence areas is a very big challenge because these systems are not sensitive enough to detect small leaks. Furthermore, detection of small volume leaks in natural gas pipelines remains a daunting task. Inspection intervals of rights-of-way and

crossings under navigable waters are mandated to pipeline operators by 49 CFR 195.412, Subpart F – Operation and Maintenance. Each operator is required to inspect the surface condition on or adjacent to each pipeline right-of-way at least 26 times in a calendar year not exceeding 3-week intervals. This is important for threat assessment.

Technology must be developed and adopted to better inspect, monitor, and manage threats at inland river crossings. Major rain events and flooding often causes depletion of cover between the riverbed and the pipeline resulting in damage. Flood events may cause damage to pipelines as a result of extreme force of the flowing water or from the pipelines being struck by heavy debris flowing down river. Active monitoring can greatly reduce the loss of product from the pipeline and avoid or minimize "environmental" damages. PHMSA identified 20 accidents occurring at inland water crossings exceeding 100 feet from high water mark to high water mark between 1991 and late 2012 (PHMSA, 2013). Of these, 16 were a result of a reduction in cover depth in either waterways or new channels cut by floodwaters as presented in Table 1. For example, seven natural gas and hazardous liquid pipelines failed as a result of major flooding near the San Jacinto River in Texas between October 19-12, 1994. Today, 49 CFR 192.613 (natural gas pipelines) and 49 CFR 192.401 (hazardous liquid pipelines) outline requirements of pipeline operators to maintain continuing surveillance of their facilities and to correct damage affecting safe operation including damage that may result from extreme flood condition. Timely leak detection to prompt an operator's response to a leak is key to threat mitigation.

Table 1. Failure of Hazardous Liquid Pipelines from Depletion of Cover at Inland Bodies of Water – 1993 to 2011 (adapted from PHMSA, 2013)

Operator	Product	Date of Occurrence
Amoco Pipeline Co.	Refined Petroleum	April 1, 1993
Williams Pipeline Co.	Highly Volatile Liquid	July 3, 1993
Exxon Pipeline Co.	Highly Volatile Liquid	October 19, 1994
Colonial Pipeline Co.	Refined Petroleum	October 20, 1994
Colonial Pipeline Co.	Refined Petroleum	October 20, 1994
Texaco Pipeline Inc.	Crude Oil	October 21, 1994
Texas Eastern Product Pipeline	Refined Petroleum	December 20, 1994
Chevron USA	Crude Oil	March 11, 1995
Conoco Inc.	Highly Volatile Liquid	October 7, 1998
Mid Valley Pipeline Co.	Crude Oil	January 26, 2005
Shell Pipeline Co. LP	Crude Oil	September 2, 2005
ExxonMobil Pipeline Co.	Refined Petroleum	June 14, 2007
Chevron Pipeline Co.	Crude Oil	December 23, 2009
ExxonMobil Pipeline Co.	Crude Oil	July 1, 2011
Nustar Pipeline Operating	Highly Volatile Liquid	July 15, 2011
Enterprise Products Operation	Refined Petroleum	August 13, 2011

PHMSA (2013) concluded that damage to pipelines occur as a result of additional stresses imposed by undermining of the support structure and by impact and/or waterborne forces. Resultant erosion causes loss of support for both buried and exposed pipelines. The increased flow of water from flooding against an exposed pipeline many also creates forces capable of causing failure. Additionally, accumulation of debris may also contribute.

Pipeline leaks in rivers often result in costly monetary losses. On September 21, 2016, ExxonMobil Corp. agreed to pay $12 million to the State of Montana and the U.S. government as a result of a pipeline rupture on July 1, 2011 that spilled oil into the Yellowstone River causing damage to natural resources. Over 63,000 gallons (238,474 liters) of crude oil was released affecting 85 miles of the flood-swollen Yellowstone River. Exxon estimated that they spent close to $135 million in cleanup and compensation to affected property owners (Reuters, Sept 21, 2016).

More recently, in January 2015, the Poplar oil pipeline spilled 40,000 gallons (151,416 liters) of oil into the Yellowstone River contaminating local water supplies and harming local wildlife. The pipeline operator, Bridger Pipeline, claimed that a 2012 inspection revealed that the pipeline was buried at a depth of 8 feet (2.4 meters) under the riverbed, which is 4 feet (1.2 meters) deeper than the minimum depth as per 49 CFR Part 195.248, Subpart D – Construction. Investigators found 120 feet (36 meters) of exposed pipeline following the spill. Depletion of cover resulting from flooding events was deemed to be responsible for the damage.

The “River Scour Monitoring System” technology will benefit society by being an “active” monitoring system capable of determining the degree of scour thereby alerting pipeline operators should the amount of cover of the pipeline become reduced. The system is intended to perform similarly on narrow and wide river systems; however, the impact from seasonal flooding is more of an issue and a threat to pipelines in narrow rivers such as those studied in this research.

2.0 REVIEW OF EXISTING THREAT PREVENTION METHODS

There are a variety of methods that can detect leaks in hazardous liquid and natural gas pipelines, ranging from manual inspection to advanced satellite based hyper-spectral imaging (Carlson, 1993). The various methods can be classified into non-optical and optical methods. The primary non-optical methods include acoustic monitoring (Hough, 1998; Klein, 1993); gas sampling (Sperl, 1991); soil monitoring (Tracer Research Corporation, 2003); flow monitoring (Turner, 1991; Bose and Olson, 1993); and software based dynamic modeling (Griebenow and Mears, 1988; Liou and Tian, 1994).

The United States Department of Transportation (USDOT) regulates the “Transportation of Hazardous Liquids by Pipeline” under federal regulations in 49 CFR Part 195. Part 195 recognizes computational pipeline monitoring (CPM) as the acceptable standard for leak detection systems on hazardous liquid pipelines, and that each CPM system must comply with American Petroleum Institute (API) Standard 1130. CPM systems employ software modeling that dynamically evaluates flow-monitoring devices measuring the rate of change of pressure or the mass flow at different sections of the pipeline. If the rate of change of pressure or the mass flow at two locations in the pipe differs significantly, it could indicate a potential leak. The major advantages of the system include its ability to monitor continuously, as well as non-interference with the operation of the pipeline. The two disadvantages of the system include the inability to pinpoint the leak location, and the high rate of false alarms. These systems are also very expensive for monitoring a large network of pipes.

In October 2016, The Norlite North Saskatchewan River project installed a 24-inch (600 mm) steel pipe and an HDPE conduit preloaded with fiber optic cables to cross a large navigable river and major source of drinking water, via a 3,160-foot (966 meter) Horizontal Directional Drilling (HDD) crossing. A fiber optic cable was simultaneous installed and placed next to the steel pipe designed to transport liquid hydrocarbons. Once turned on, this has the potential for adding an additional layer of active leak detection in high consequence areas such as river crossings. Incidentally, one suggestion for safeguarding crossings is to replace trenched crossings with HDD installations (PHMSA, 2016). Although a novel concept, it only addresses new installations and not existing pipelines already in service.

3.0 RIVER SCOUR MONITORING SYSTEMS (RSS)

3.1 Introduction

The River Scour Monitoring Systems (RSS) is based on a temperature gradient decay method for monitoring a subject pipeline river crossing for scour conditions. In simplified terms, the monitoring system consists of the installation of high accuracy temperature sensors on the pipeline on either side of the crossing, and in close proximity to it. The temperature gradient as a function of distance would be established based on two upstream sensor inputs. That gradient is used to predict the temperature at the downstream sensor location based on its distance from the upstream sensor. Any variance between the predicted and actual measured temperatures at the downstream location would be as a result of an anomalous thermal loss (or gain) between the upstream and downstream sensors, which would be indicative of reduced cover due to scour through to full exposure of the pipeline, resulting from the dramatically higher thermal conductivity of the water. The general field configuration of the "River Scour Monitoring System" is illustrated in Figure 1.

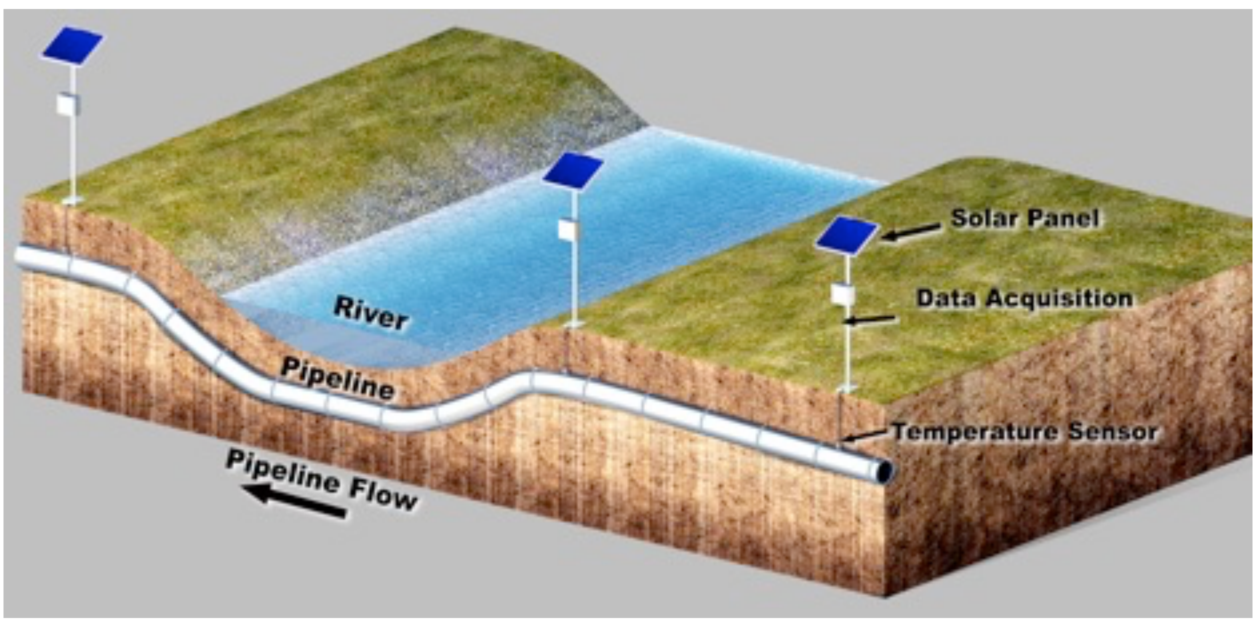

Figure 1. Configuration of River Scour Monitoring Systems (RSS)

3.2 Installation

We installed monitoring systems at five (5) demonstration sites to assess the viability of the "River Scour Monitoring System". The sites were divided between Canada and the United States to maintain a breadth of geological and environment conditions. Data was collected daily, using remote communication, from each of the sites to enable continuous monitoring and analysis to assess the competency of the monitoring system. The intent was to have between 12 to 18 months of collected data for analysis from each demonstration site. The goal was to leverage the prototype technology and knowledge gained from this proposed project to develop a commercially available tool for the hazardous liquids and natural gas pipeline industry that will be available within the next two to three years. A prototype RSS System was installed at a Kinder Morgan site in British Columbia, Canada in 2016 as shown in Figure 2.

Figure 2. Prototype River Scour Detection System at Kinder Morgan Site

Data collected and analyzed from the first demonstration installation has validated the proof of concept as indicated in Figure 3.

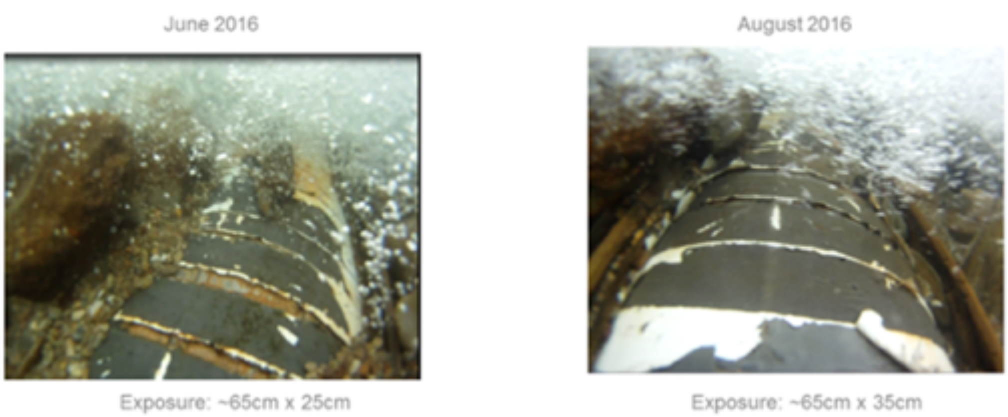

Figure 3. Exposure (due to river scour) of Pipeline at Kinder Morgan Demonstration Site

4.0 SITE INSTALLATIONS

4.1 Introduction

River Scour Monitoring Systems (RSS) were installed on four oil pipelines owned and operated by Enbridge Pipelines at two different river crossing sites of the Tongue River Crossing, North Dakota and Elk River Crossing, Kansas; and one oil pipeline owned and operated by Pembina Pipelines at the Freeman River Crossing, Alberta. These were performed by trained technicians and provided an opportunity to evaluate the novel RSS systems. Location selection for this research was primarily driven by operational partner constraints and shallow cover potential.

4.2 Tongue River Crossing, North Dakota

The Tongue River, shown in Figure 4, is a 145 km (90 mile) long tributary of the Pembina River in northeastern North Dakota. In this area, the pipelines run from northeast to southwest. The installations on the Tongue River occurred from November 18-20, 2019, on two parallel pipelines. Three sensors were placed on each pipeline, two upstream and one downstream of the Tongue River. Table 1 and Table 2 present the sensor installation locations. Due to relative ease of site access, conventional trenching methods were used to expose the pipeline at the riverbank for the sensor installation (Figure 5). Figure 6 provides and aerial view of the installation. The completed above ground monitoring systems are shown in Figure 6.

Figure 4. Tongue River Crossing

Figure 5. Sensor Installation at Tongue River

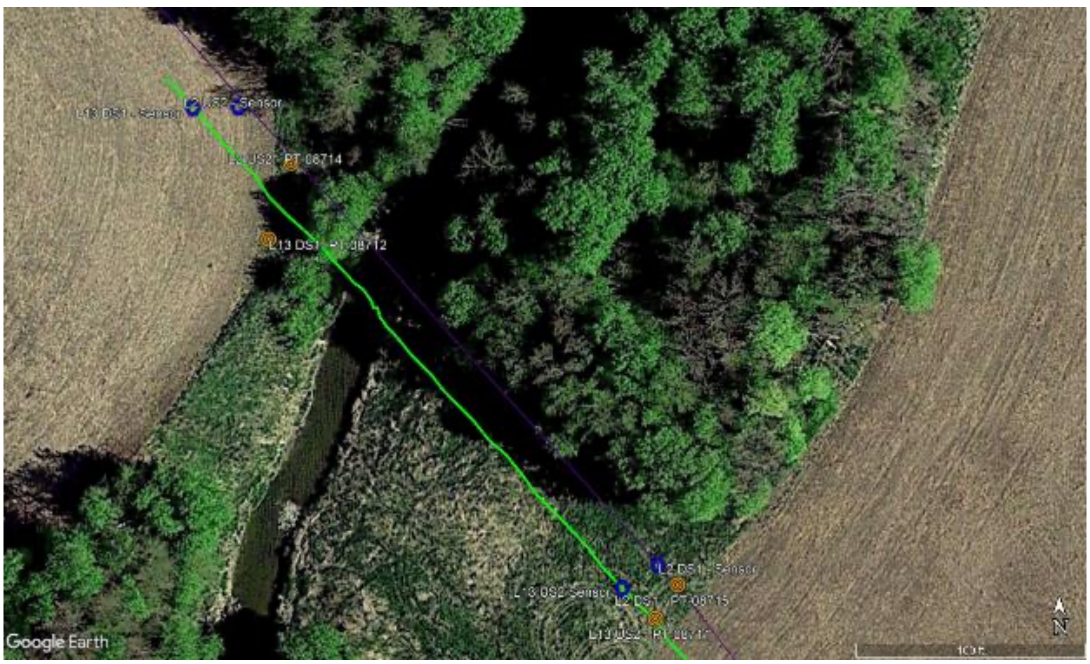

Figure 6. Tongue River Site Overview

Figure 7. Tongue River Scour System Above Ground Equipment

Table 2. Tongue River Sensor Installation Locations - Line 2

Location	Sensor	Latitude (deg)	Longitude (deg)	Distance (ft)
Upstream 1	PT-08710	48.86192	-97.341295	0
Upstream 2	PT-08711	48.867426	-97.34882	2706.36
Downstream 1	PT-08712	48.867996	-97.349597	3004.92

Table 3. Tongue River Sensor Installation Locations - Line 13

Location	Sensor	Latitude (deg)	Longitude (deg)	Distance (ft)
Upstream 1	PT-08713	48.87648	-97.361031	0
Upstream 2	PT-08714	48.867997	-97.349515	4156.5
Downstream 1	PT-08715	48.867453	-97.348755	4443.24

4.3 Elk River Crossing, Kansas

The Elk River is a tributary of the Verdigris River in southeastern Kansas. Enbridge Lines 55 and 59 cross the river to the northwest of Independence, Kansas just downstream of the manmade Elk City Reservoir (Figure 8). Due to site access and the depth of cover on the pipeline, the sensors were installed using a potholing method (Figure 9). The installations on the Elk River took place from December 3-7, 2019.

The depth of cover varies greatly between the two lines due to the different construction vintages. Line 55, built in the 1950s, has a depth of cover around 600 mm to 1,200 mm (4 to 6 feet) in the general right of way and lowers to 4.57 m (15 feet) near the river crossing. Line 59, built in the 2000s, has a depth of cover between 1,800 mm and 2,100 mm (6 and 7 feet) in the general right-of-way (ROW) and was directionally drilled underneath the Elk River and is extremely deep. The depth of cover on Line 59 at the river crossing is greater than 18 m (60 feet), therefore we did not install a sensor on Line 59 near the Elk River and instead elected to install one near the downstream valve. An extra sensor was installed on Line 55 in order to have one installed as close to the river as possible and one near the downstream valve to be comparable to the Line 59 system shown in Figure 10. The sensor locations are presented in Table 4 and Table 5. These are also illustrated in Figures 11 – 14.

Figure 8. Elk River Crossing

Figure 9. Elk River Crossing Sensor Installation

Figure 10. Elk River Above Ground Equipment

Table 4. Elk River Sensor Installation Locations - Pipeline 1

Location	Sensor	Latitude (deg)	Longitude (deg)	Distance (ft)
Upstream 1	PT-08720	37.28353	-95.72998	0.00
Upstream 2	PT-08716	37.27664	-95.73273	2634.28
Downstream 1	PT-08718	37.26894	-95.73607	5615.45

Table 5. Elk River Sensor Installation Locations - Pipeline 2

Location	Sensor	Latitude (deg)	Longitude (deg)	Distance (ft)
Upstream 1	PT-08722	37.28355	-95.72979	0.00
Upstream 2	PT-08717	37.27664	-95.73254	2639.07
Downstream 1	PT-08719	37.26904	-95.73581	3419.91
Downstream 2	PT-08721	37.27454	-95.73281	5625.16

Figure 11. Elk River Upstream Sensor 1 Site Overview

Figure 12. Elk River Upstream Sensor 2 Site Overview

Figure 13. Elk River Downstream Sensor Site Overview

Figure 14. Elk River Downstream Sensor 2 Site Overview

4.4 Freeman River Crossing, Alberta

Installation was completed from March 7-11, 2020 on a 400 mm (16-inch) pipeline owned and operated by Pembina Pipelines under the Freeman River near Fort Assiniboine, Alberta Canada. The Freeman River is a relatively short tributary of the Athabasca River that flows in the southeastern direction from Swan Hills, Alberta to Fort Assiniboine, Alberta. Normally, the river experiences low flow and is not very deep; however, it is prone to large flooding events during spring run-off and during rains. The river crossing at the time of install is shown in Figure 15.

Three sensors were placed on the pipelines: two upstream and one downstream. One of the River Scour Monitoring Systems (RSS) was placed to monitor a buried pipeline, while the other was placed to monitor a parallel exposed pipeline. This provided an excellent comparison of the operation efficiency of the RSS. The pipeline was exposed and recoated using conventional trenchless pipeline repair methods. Figure 16 shows the sensors after being epoxied to the pipe at each location and Figure 17 shows the above ground installed RSS units at each location.

Figure 15. Freeman River Crossing in March 2020

Figure 16. Sensor Installations at the Freeman River from Left to Right: Upstream 1, Upstream 2 and Downstream 1

Figure 17. Above Ground River Scour Monitoring Systems at the Freeman River from Left to Right: Upstream 1, Upstream 2 and Downstream 1

5.0 FIELD DATA COLLECTION

Daily data collection (every 10 minutes) and monthly analysis was conducted for the installations at the Tongue River, Elk River, and Freeman River sites installed in November (2019), December (2019) and March (2020), respectively. Temperature data on the pipe, soil and air as well as a battery voltage were collected every ten minutes at each sensor location since installation. Sample data for the five installations is found in Appendix A. Currently, the data is viewed on the PureHub (a proprietary software) with an interactive graph and downloaded as an excel spreadsheet.

5.1 Tongue River Crossing, North Dakota

The Tongue River system was installed between November 18 - 20, 2019. Two pipelines are currently being monitored for temperature changes. Data from December 2019 to July 2021 (19 months) on Pipeline #1 and Pipeline #2 are presented in Figure 18 and Figure 19, respectively. Both pipelines showed a close temperature alignment between the upstream and downstream RRS units. These results indicate that no river scour concerns are currently present on these pipelines. Pipeline #1 had temperatures ranging from 3°C to 18°C, while Pipeline #2 ranged from 8°C to 22°C.

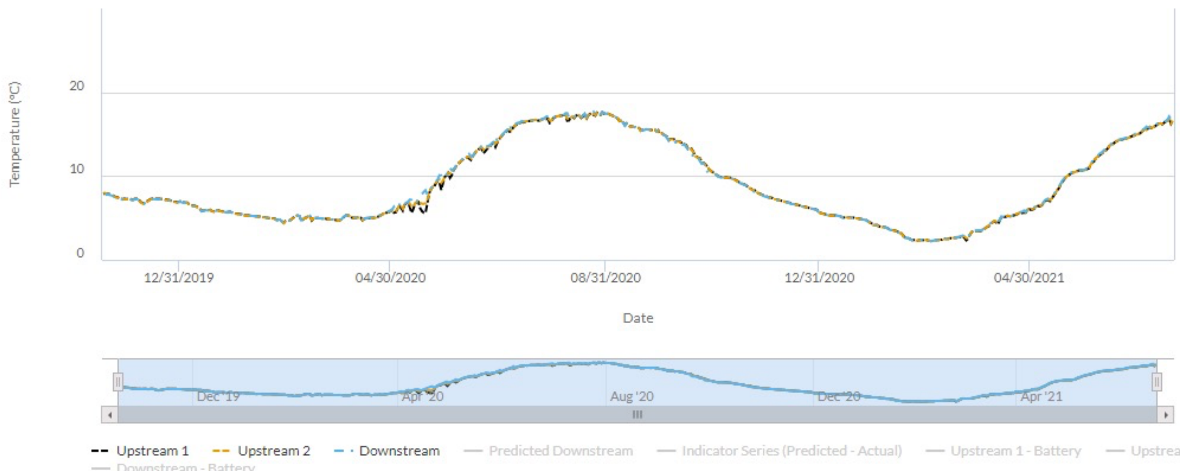

Figure 18. Pipeline Temperatures on Tongue River Pipeline #1

Figure 19. Pipeline Temperatures on Tongue River Pipeline #2

5.2 Elk River Crossing, Kansas

The Elk River system was installed between December 3-7, 2019 in Kansas. Two pipelines are currently being monitored for temperature changes. Pipeline #1 was installed in the 1950's using open cut construction to cross the river. Pipeline #2 was installed in the 2000's using Horizontal Directional Drilling under the river. Temperatures from the RSS units from December 2019 to June 2021 (18 months) for Pipeline #1 and #2 are presented in Figure 20 and Figure 21, respectively. Pipeline #1 exhibited a close temperature alignment between the upstream and downstream RRS units; however, Pipeline #2 revealed slight deviation between the upstream and downstream RSS units. Pipeline #1 had temperatures ranging from 10°C to 28°C, while Pipeline #2 ranged from 5°C to 30°C.

As part of the monitoring program, a crew was sent to the Elk River to collect bathymetric and depth of cover data to assess the amount of cover on the pipelines. Bathymetry was collected using a high-resolution multi-beam sonar to create a map of the river channel bottom shown in Figure 22. There was no indication that the pipeline was exposed under the water. Depth of cover data was also collected by impressing an AC current on the pipeline and calculating the depth of pipe by measuring the strength of the induced electromagnetic field. Figure 23 shows the profile and plan of Pipeline #2 at the Elk River crossing. The pipeline was not exposed; however, it was found to have shallow depth of cover in the water channel, which could explain the temperature differentials between the upstream and downstream RSS units shown in Figure 16. This pipeline is continually monitored for possible future river scour.

Figure 20. Pipeline Temperatures on Elk River Pipeline #1

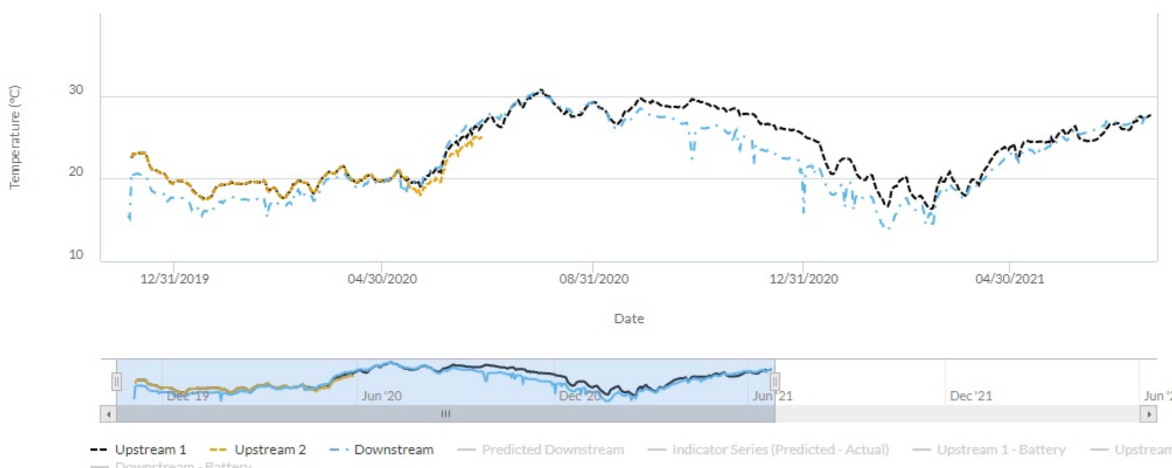

Figure 21. Pipeline Temperatures on Elk River Pipeline #2

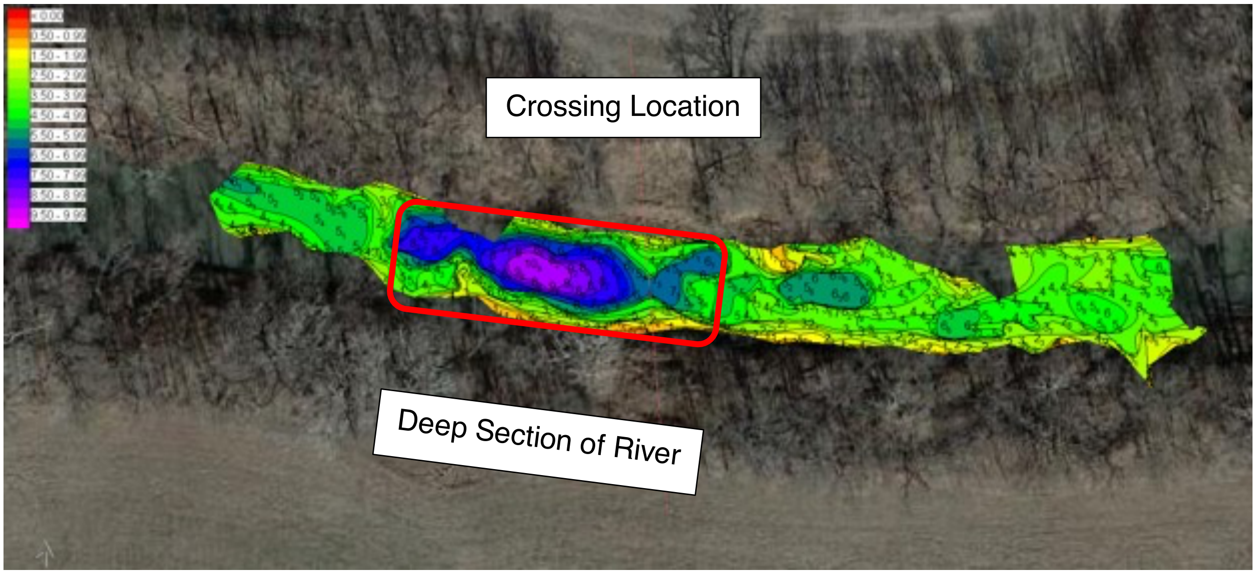

Figure 22. Elk River Crossing Bathymetry

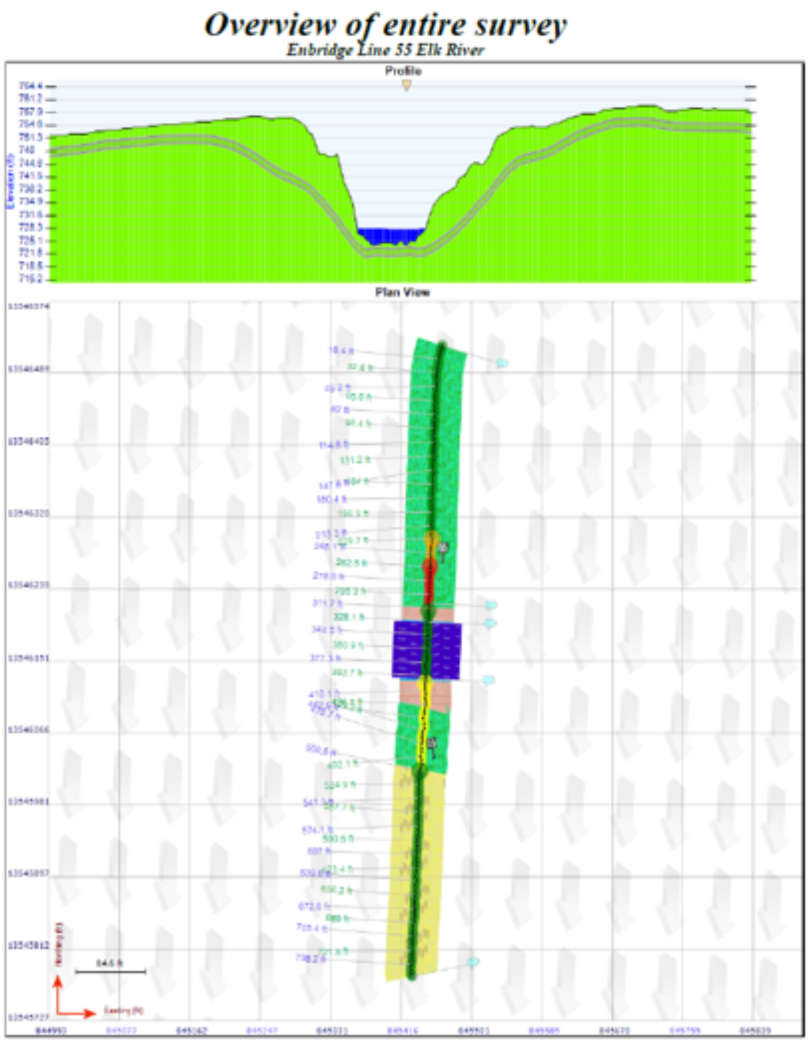

Figure 23. Elk River Crossing Plan and Profile

5.3 Freeman River Crossing, Alberta Canada

The Freeman River system was installed on March 7-11, 2020, on a 400 mm (16 inch) pipeline near Fort Assiniboine, Alberta, Canada. Temperature data collected from March 2020 to July 2020 (4 months) are illustrated in Figure 24. The pipeline exhibited a close temperature alignment between the upstream and downstream RRS units. Unfortunately, on July 5th, 2020, the downstream unit was severely damaged and torn down by vandals and stopped communicating. It was assessed that it could not be repaired without re-exposing the pipeline. The two upstream RSS units continued to collect data until the system was fully decommissioned in February 2021 after the pipeline crossing was replaced. The pipeline had temperatures ranging from 4°C to 15°C. The pipeline right-of-way is shown in Figure 25.

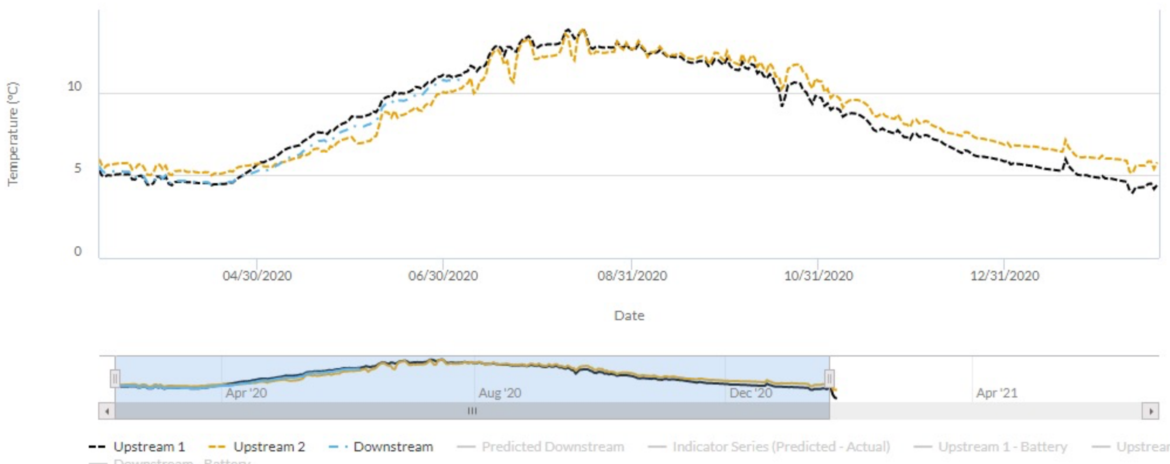

Figure 24. Pipeline Temperatures on Freeman River Pipeline

Figure 25. Pipeline Right-of-Way on the Freeman River Pipeline

A camera system was installed in April 2020 to take daily pictures to monitor the river condition throughout the winter melt and subsequent flooding. Figure 26 shows the Freeman River on May 5, 2020, with high water levels. In June 2020, after some high river levels, a potential scour was identified during analysis of the data. A crew was mobilized with a high-resolution multi-beam sonar device, shown in Figure 27, to map the bottom of the river to verify a pipe exposure. After analysis, it was determined that the pipe area exposed to water was only 0.79 m^2. This will need to be monitored.

Figure 26. Freeman River Pipeline Crossing from the Installed Camera System (May 2020)

Figure 27. Survey Boat Containing High-Resolution Multi-Beam Sonar

6.0 SOFTWARE AND HARDWARE

6.1 Software/Website Upgrade

Four versions of the desktop software and website were completed during the project. Version 1.0 is capable of visualizing data from the RSS sensors. In version 1.0 the functionality of the software was limited to: viewing the device location, grouping the devices into sites, entering a device specific linear calibration formula and browsing the data. Users at the time were unable to directly download the sensor information. A cumbersome process involving converting the raw data from binary into readable data was used. Figure 28 illustrates the high-level operating diagram of the software.

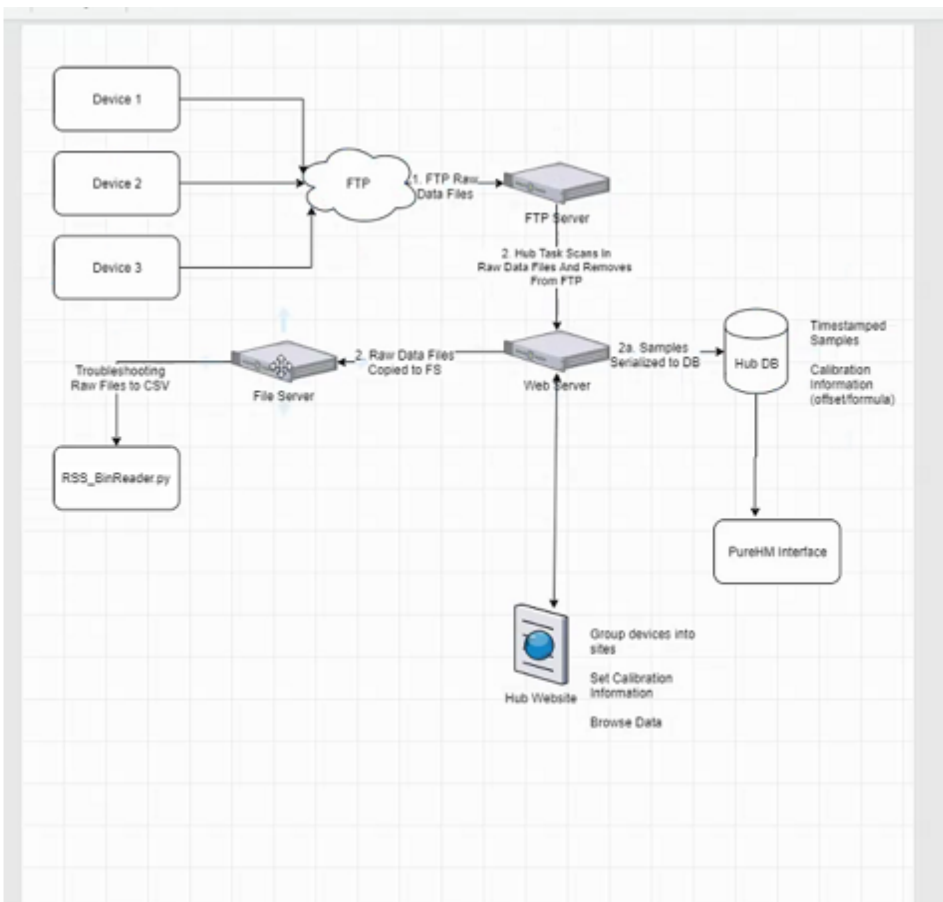

Figure 28. Software Operating Diagram (Version 1.0)

Version 2.0 was upgraded to enable the RSS units being installed and monitored to be pre-loaded on the website. The input screen is illustrated in Figure 29. To go along with upgraded sensor hardware, users are now able to enter custom polynomial sensor calibration on various channels as shown in Figure 30. Version 2.0 also included upgrades to the Pure Hub, where users could interact with the data, using sliders along the bottom of the screen to change date ranges, zoom in on areas of interest, and turn on and off different sensor channels. The Version 2.0 Hub display is shown in Figure 31. Functionality was also added to give users the ability to download data directly off the Hub site into excel.

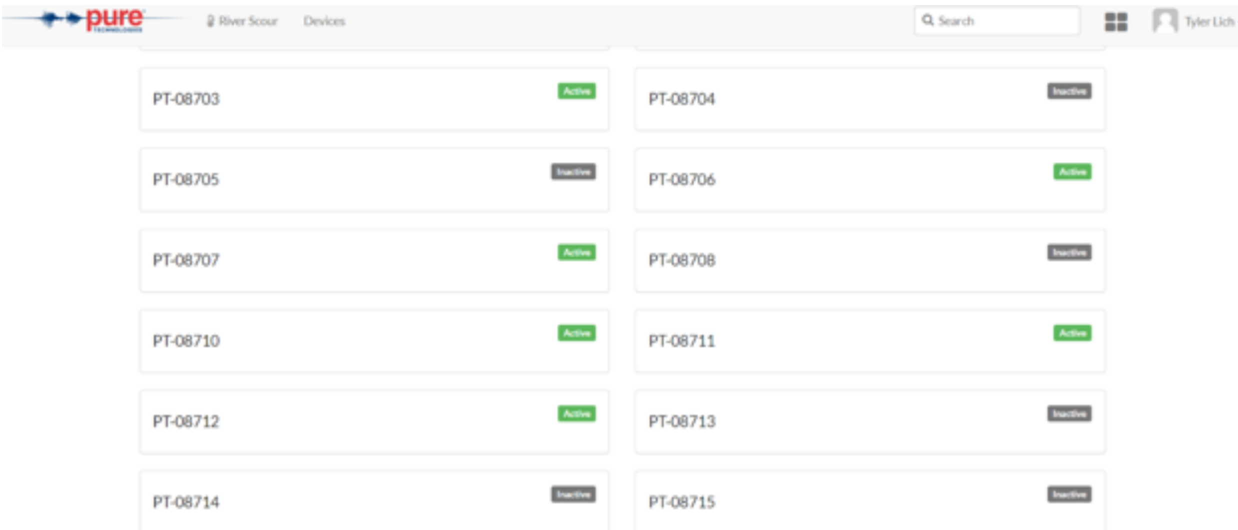

Figure 29. Input Screen for RSS Monitoring (Version 2.0)

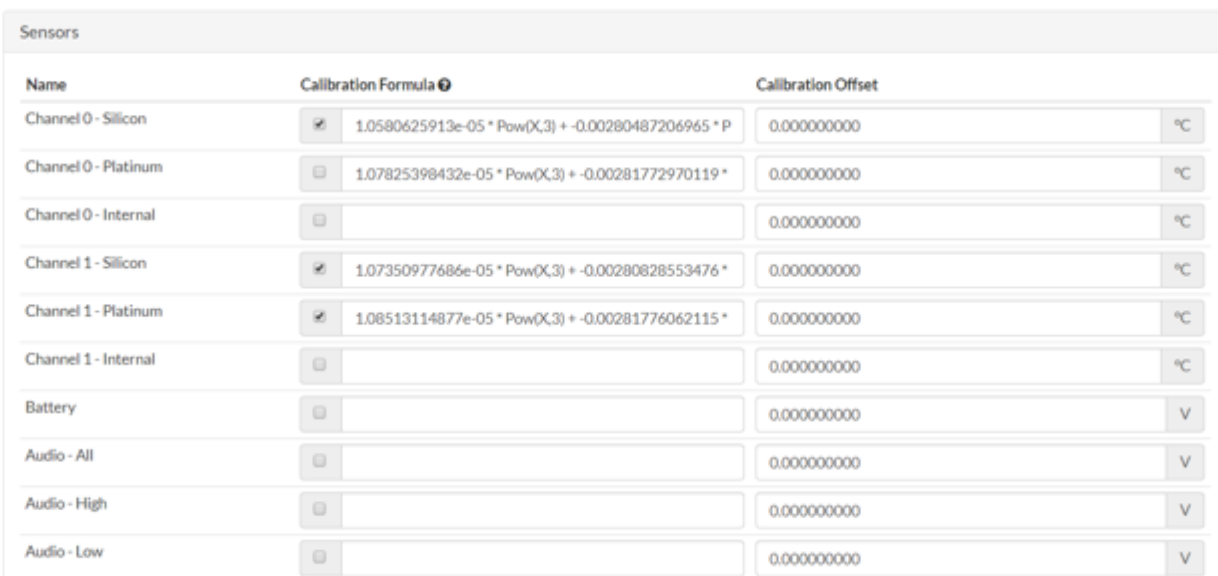

Figure 30. Custom Sensor Calibration (Version 2.0)

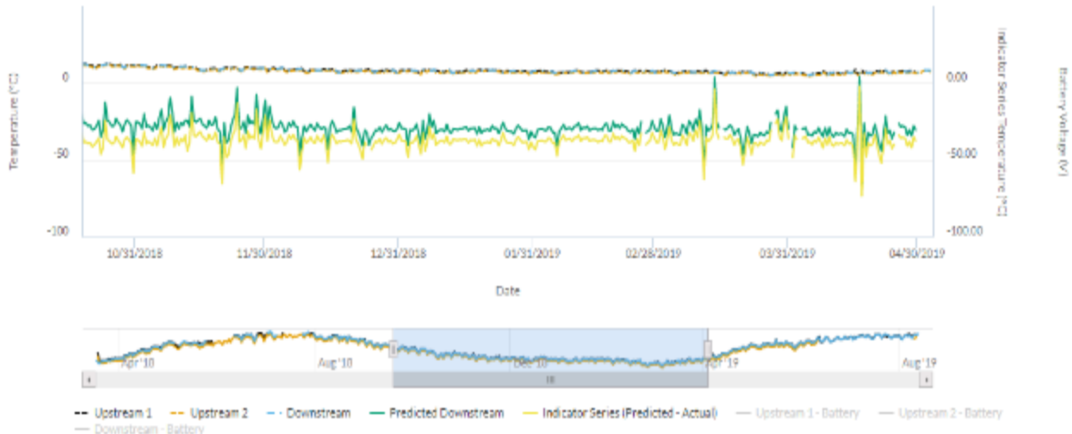

Figure 31. Pure Hub Display Software Upgrade (Version 2.0)

Significant progress was made in Version 3.0 towards integrating the RSS system into the greater Xylem sensor suite via development of the RTT. The communications board developed for the RTT was integrated into new versions of the RSS system allowing it to communicate via cellular, satellite and FlexNet. This gives users more flexibility when choosing what to install on their pipeline system. Which is an improvement on the current iteration of the RSS that can only communicate via satellite signals. While satellite is a robust method of data transmission, it can be costly to operate.

Version 3.0 of the software allowed for integration of the operators SCADA pressure data in a more easily viewed format, as shown in Figure 32. Additionally, the RSS Software was upgraded to create an adaptive algorithm to optimize the pipe sensor bias correction. Previously, the software used 4 bias correction parameters to account for environmental or calibration errors. Since the ground temperature was found to be generally quite stable and consistent across sections, we eliminated the reliance on ground sensors to remove 2 biases. Now using overall heat transfer ratios to set a “scour threshold” that can be set to alarm when the system crosses it, seen in Figure 33.

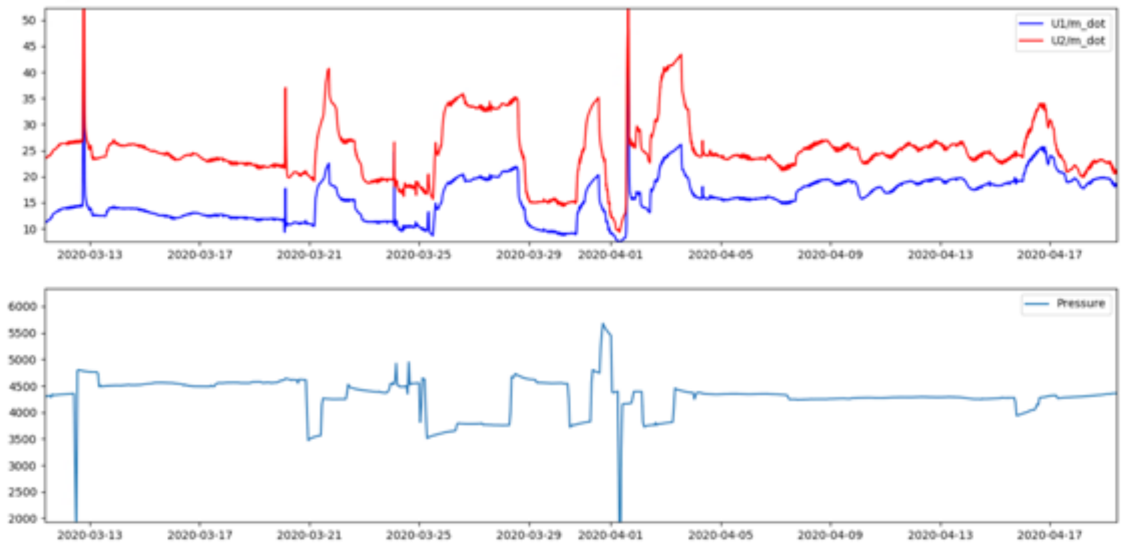

Figure 32. Correlation with SCADA Pressure Data (Version 3.0)

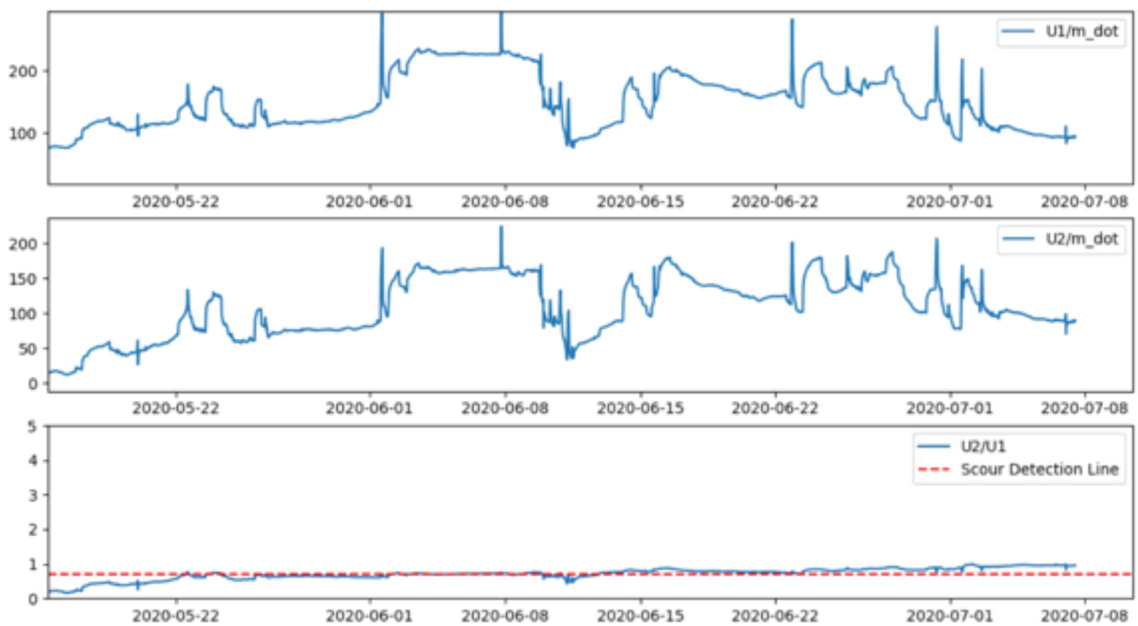

Figure 33. Auto Bias Adjustment and Scour Detection Threshold (Version 3.0)

Version 4.0 of the software upgrade includes the creation of a client specific login page. Previously all data was hosted on one page on the Hub and for confidentiality reasons login information was not distributed to multiple operators. Now multiple operators can view their river crossings without the ability to see competitor's river crossing information. Also, with the incorporation of a camera into the system, the software now enables hosting of those images on the same site that the RSS information is currently on.

Version 4.0 also incorporated the Jupyter Notebook (Figure 34) to make processing easier for analysts to calculate overall heath transfer coefficient (OHTC) and mass flow rates. Jupyter Notebook is an open-source web application that enables the user to create and share documents that contain live code, equations, visualizations, and narrative text. The notebook serves a dual purpose of a walkthrough for data processing as well as live code to create visualizations for analysis.

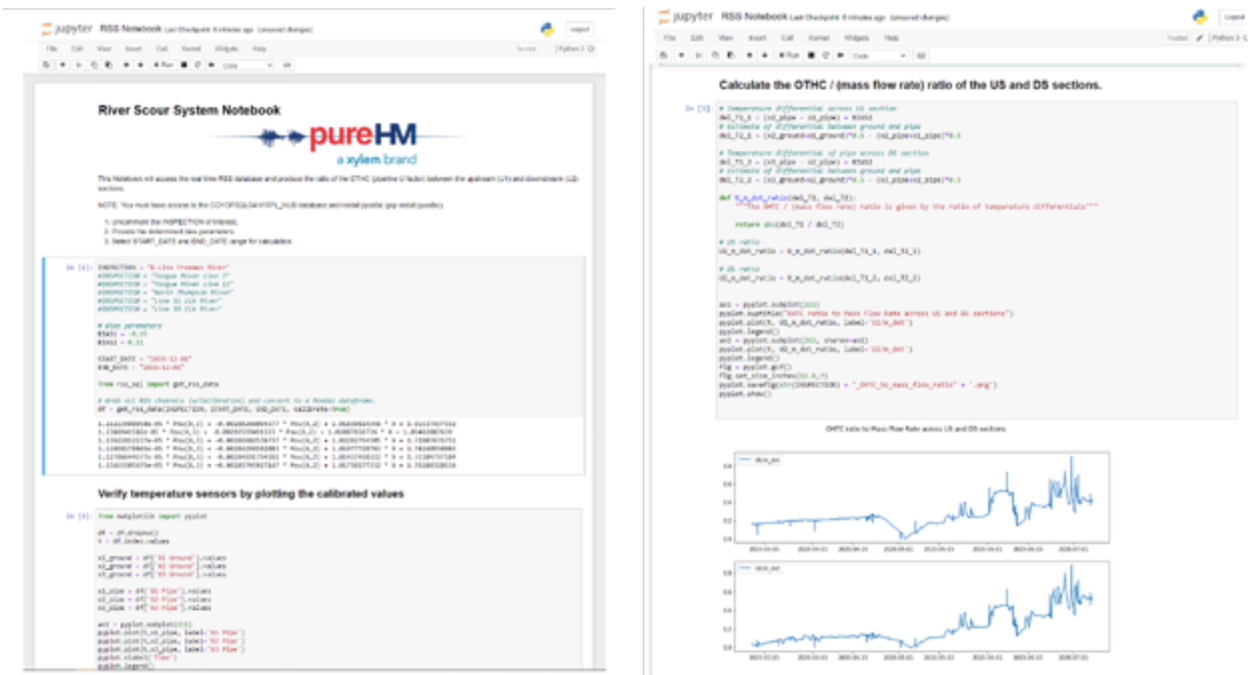

Figure 34. Incorporation of Jupyter Notebook Source (Version 4.0)

6.2 River Scour Monitoring System Hardware Upgrade

Version 1.0 RSS was rudimentary in design and did not contain solar panels for power thereby requiring charging every few months. The initial units had a buried pipe and soil sensor and were pole mounted. Additionally, there was no regulatory certification for the Version 1.0 unit. The schematic drawings of Version1.0 is shown in Figure 35.

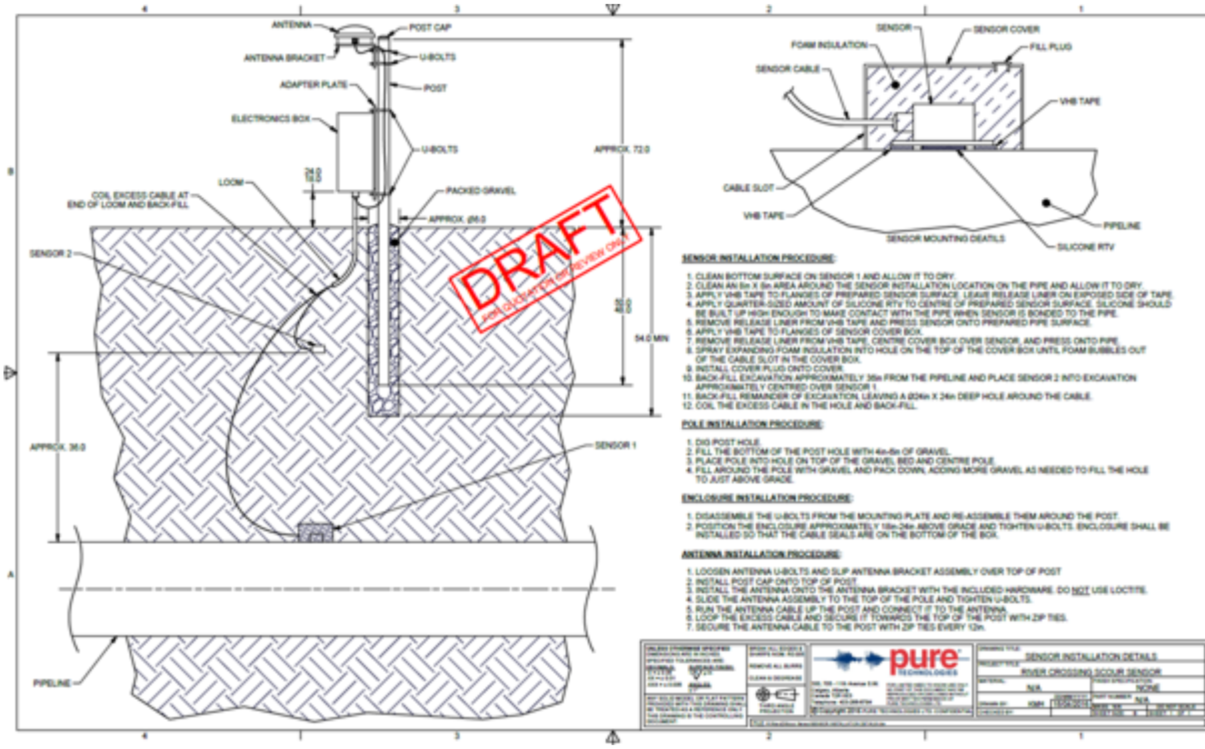

Figure 35. Schematic Drawings of Version 1.0 RSS Units

Solar Panels were added for Version 2.0, which also contained a more robust electronics enclosures as shown in the schematics in Figure 36. The temperature sensors were upgraded to a more sensitive multi-channel silicon sensor. Also, an active pod was added containing a magnetometer and accelerometer to be placed directly on the existing pipe. A buried slack cable box was included along with conduit to contain the sensor cables. Figure 37 illustrates the sensor installation details.

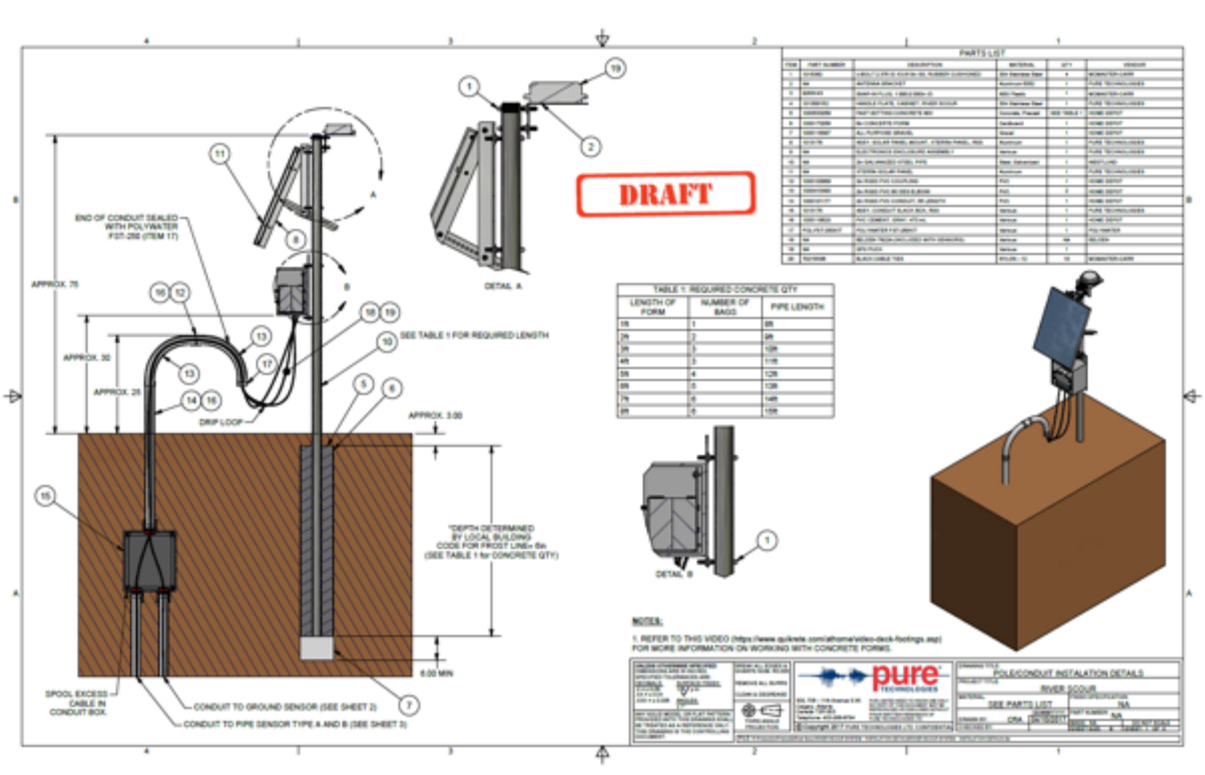

Figure 36. Schematic Drawings of Version 2.0 RSS Units

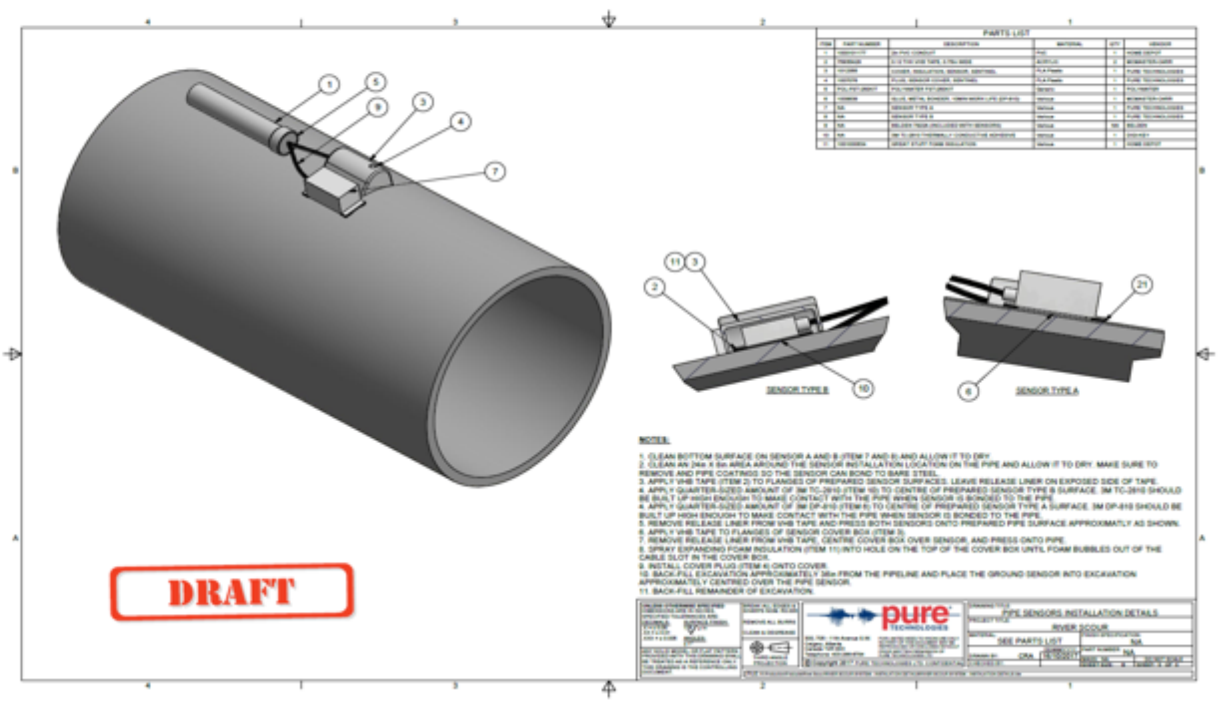

Figure 37. Pipe Sensor Installation Details

The Version 3.0 system contained several mechanical improvements including moving the slack cable box above ground, using direct burial cables with reinforced conduit at the soil-air transition, and a semi-permanent, non-intrusive base (Figure 38 & 41) in addition to the pole burial (Figure 40). On the electrical side, a solar charger was integrated into the main PCB of each system (Figure 39). Thirty-five Version 3.0 RSS systems were manufactured and tested, sixteen were installed on operating pipelines across North America.

Regulatory certification to the following standards were obtained for Version 3.0:

- Safety Requirements for Electrical Equipment for Measurement, Control, And Laboratory Use - Part 1: General Requirements [UL 61010-1:2012 Ed.3]
- Safety Requirements for Electrical Equipment for Measurement, Control, And Laboratory Use Part 1: General Requirements [CSA C22.2#61010-1-12:2012 Ed.3]
- Nonincendive Electrical Equipment for Use in Class I And II, Division 2 And Class III, Divisions 1 And 2 Hazardous (Classified) Locations [ISA 12.12.01:2016 Ed.7]
- Nonincendive Electrical Equipment for Use in Class I And II, Division 2 And Class III, Divisions 1 And 2 Hazardous (Classified) Locations [CSA C22.2#213:2016 Ed.2]

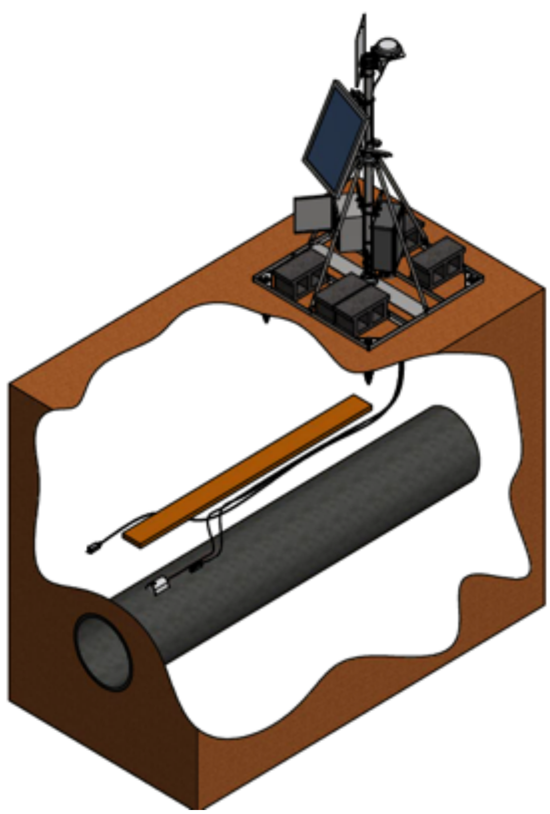

Figure 38. Version 3.0 Mechanical Configuration Upgrades

Figure 39. Version 3.0 Electrical Configuration Upgrades

Figure 40. Version 3.0 Pole Mounted Installation

Figure 41. Version 3.0 Tripod Mounted Installation

Version 4.0 involved integrating a camera (Figure 42) into the system to provide a visual indication of the river status. Consideration was taken to build this directly on the RSS monitoring installation, but for the most part, they had obstructed views of the river. Therefore, the camera serves as a standalone piece for optimal viewing of the river.

Figure 42. Version 4.0 RSS Camera Addition

To reduce the risk of third-party damage to the RSS units, Version 5.0 offered more robust steel conduit and enhanced perimeter security fencing (Figure 43) was placed to provide a deterrent to future potential damage. This physical barrier is necessary as many of these crossings are in remote areas where the installed RSS units are vulnerable. This was deemed necessary after the vandalization of the RSS unit installed at the Freeman River Crossing in Alberta.

Figure 43. Version 5.0 RSS Unit with Enhanced Security Measures

7.0 VORTEX-INDUCED VIBRATION (VIV)

7.1 VIV Background

However, one of the more ominous threats is known as "Vortex-Induced Vibration (VIV)" that, once started, can result in pipeline failure within hours in the more severe cases with vibration amplitudes equal to the diameter of the pipe being possible. Fluid flow perpendicular to a free span pipeline's longitudinal axis will result in the formation and shedding of vortexes. This effect induces an oscillating vibration motion on the pipeline, perpendicular to the water flow and the pipeline axis; in the case of inland water crossings this will typically be a vertical oscillation. The phenomenon can be responsible for subjecting a pipeline to hundreds of thousands of unexpected pressure cycles per day and result in very premature failure.

As such, detection of VIV conditions being present on a pipeline is of particularly urgent concern to geohazard management groups. Since a free-span condition of the pipeline is one of the pre-requisites for VIV to form, a real-time monitoring system capable of detecting the reduction of pipeline cover through river scour should be an effective means of mitigating concerns related to VIV by detecting exposed and free-span pipe as it happens. A Finite Element Model (FEM) was developed to help determine the length of free span that would make a given pipeline susceptible to VIV. Conducting FEM in advance will reduce pipeline damage. Active monitoring can greatly reduce the loss of product from the pipeline and avoid or minimize "environmental" damages.

In this study, a simulation model of an oil pipeline exposed on a riverbed was created, and the volume of fluid (VOF) and user defined functions (UDFs) methods in FLUENT were used to study the influence of the pipeline under the VIV of the fluid.

By probabilistic formulation and entropy maximization, Chiu et al. (1988) derived a two-dimensional velocity distribution in the form.

$$u = \frac{u_{\max}}{M} \ln\left[1 + (e^M - 1) \cdot \frac{y - y_0}{y_{\max} - y_0}\right] \tag{1}$$

Where *u* = velocity in the longitudinal direction (i.e., X-direction); M=2.13, a entropy parameter, could be adopted constant within the two river reaches investigated, whereas u_{max} was assumed as the maximum value of the velocity points sampled during each event, and the relation between the mean velocity, u_m, and the maximum velocity, u_{max}, can be expressed as $u_m = 0.665u_{max}$ (Tommaso Moramarco et al., 2004); $(y-y_0)/(y_{max}-y_0)$ represents the cumulative probability function, in which *y* is a function of the spatial coordinates in the physical space; y_{max} = *y* at the point where u_{max} occurs; y_0 = *y* at the point where *u* = 0 (here, y_0 is the spatial coordinates of the riverbed); Based on the results of Moramarco et al. (2004), y_{max}, y_0 and the flow depth D_f

basically satisfy the relation of $(y_{max} - y_0)/D_f = 0.5$. It shows that Eq. 15 performed better in the middle portion of the flow area (de Araújo and Chaudhry, 1998).

When $y < y_0$, $u = 0$; when $y \geq y_0$, Eq. 15 is used for calculation of the velocity of the water above the riverbed at different depths. Here 1.8 m/s, 2.2 m/s and 2.6 m/s are chosen as the mean velocity u_m of the fluid (see Table 3.4). UDFs is used to impose close-to-real velocities to the fluid. The specific velocity distribution form is shown in Figures 44-46.

Table 6 lists the model numbers and corresponding working conditions in this study. It has been reported that the maximum response amplitude takes place at the larger Reduced velocity V_r, which is a dimensionless parameter defined as $V_r = u/(f_n D)$, consisting of fluid velocity u, the natural frequency f_n and outside diameter D of the cylinder pipe (Tsahalis, 1984; Tsahalis and Jones, 1981). The Reynolds number R_e, defined as $R_e = \rho u_m D/\mu$, helps predict flow patterns in different fluid flow situations, which consists of the fluid density ρ, the fluid viscosity μ, the fluid mean velocity u_m, and the outside diameter D of the cylinder pipe. Based on the chosen mean velocity u_m of the fluid, V_r number and R_e number are obtained and presented in Table 6.

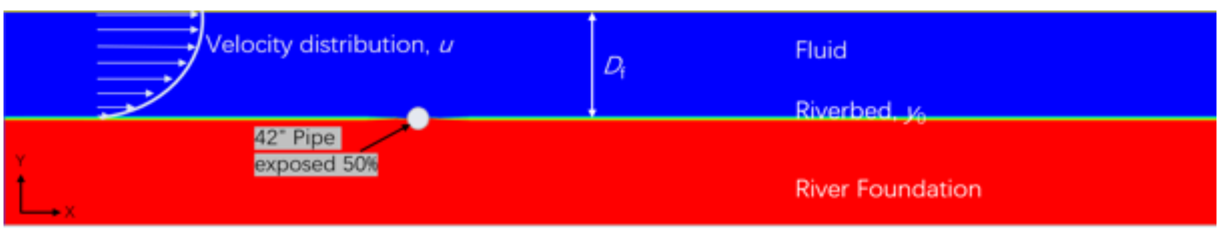

Figure 44. Velocity Distribution with Pipe Exposed 50%

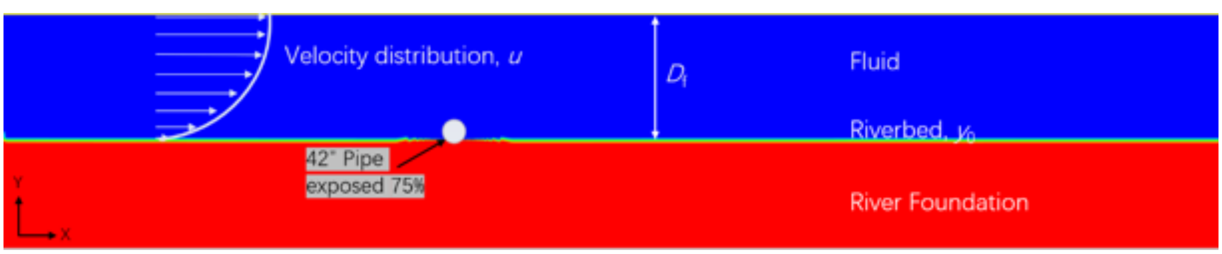

Figure 45. Velocity Distribution with Pipe Exposed 75%

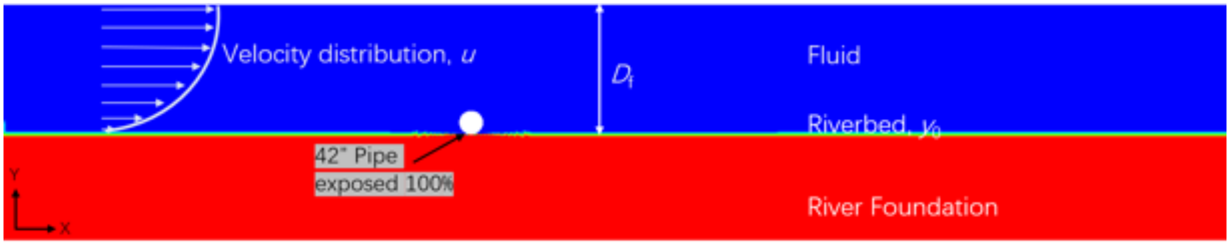

Figure 46. Velocity Distribution with Pipe Exposed 100%

Table 6. Model Number and Conditions

Model No.	*D* (m)	u_m (m/s)	Exposure Rate	V_r	R_e ($\times 10^6$)	Type of Vibration
M1	1.0668	1.8	50%	0.2362	1.911	X and Y
M2	1.0668	2.2	50%	0.2887	2.335	X and Y
M3	1.0668	2.6	50%	0.3412	2.760	X and Y
M4	1.0668	1.8	75%	0.2362	1.911	X and Y
M5	1.0668	2.2	75%	0.2887	2.335	X and Y
M6	1.0668	2.6	75%	0.3412	2.760	X and Y
M7	1.0668	1.8	100%	0.2362	1.911	X and Y
M8	1.0668	2.2	100%	0.2887	2.335	X and Y
M9	1.0668	2.6	100%	0.3412	2.760	X and Y

7.2 Phase change of multiphase flow

According to the volume of fluid (VOF) method introduced previously, FLUENT can record in real-time the change characteristics of the riverbed and the water flow and the interface between them in the process of fluid flow. Here, the phase diagrams of the key moments in the results of M1-M9 are extracted and listed in Figures 47–55, respectively.

As can be seen from the changes in these phase diagrams, regardless of the initial exposure rate of the pipe or the velocity of the fluid, as water flows through the pipe area for a period, the riverbed soil around the pipe is dispersed, resulting in the pipe complete exposure to the fluid. It is just that the time for the pipe to be fully exposed varies with different exposure rates and different flow rates.

According to the report of Thusyanthan et al. (2014), the local scour below a pipeline is a common cause for creation of free spans. The scouring process beneath a pipeline can be categorized into five key stages: onset of scour, tunnel erosion, lee-wake erosion, equilibrium stage, and scour lateral growth. As can be seen from the changes in the phase diagrams of M1-M6 (Figure 46-54), with the fluid flows through the pipe, a seepage and erosion are created at the position of the interface between the pipe and the riverbed due to the pressure difference between upstream and downstream sides of the pipe (Stage 1 - onset of scour); as seepage and erosion continue, the interface is eventually penetrated by fluid and a gap between the pipe and riverbed is created, which leads to scouring beneath the pipe (Stage 2 - tunnel erosion); next, the pipe start to vibrate in the Y-direction (i.e., lift-direction) and X-direction (i.e., drag-direction), which bring more erosion and scouring at bottom and downstream of the pipe (Stage 3 - lee-wake erosion). The difference is that the scour at downstream is not as high, which means that the vortex shedding at the end of the pipe is not obvious enough to cause a higher scour; the scouring process finally reaches a steady state in which the riverbed shear stress beneath the pipe becomes constant and the deformation of the riverbed stabilizes (Stage 4 - equilibrium stage); then the scour will develop horizontally along the pipe axis (Stage 5 - scour lateral growth).

Further observation shows that a relatively deep scour pit is formed at the bottom of the pipe around 6 seconds; there is accumulation of riverbed soil near the downstream of the pipe; the height of the riverbed near the upstream of the pipe have different degrees of reduction caused by scouring. These phenomena are very close to the experimental results of Sumer et al. (1988), Yang et al. (2013) and Gao et al. (2006), indicating the accuracy of the model and results in this study.

In addition, the changes of the phase diagrams in Figures 50, 51, 53 and 54 show different characteristics. In these models, the riverbed soil around the pipe is rolled up in a large area, and it forms a semi-enclosing vortex at the downstream of the pipe. The fluid is gyrating and flowing to upstream as it passes through here, causing the riverbed at the upstream of the pipe to be eroded more deeply. With the fluid rolls up the riverbed soil around the pipe in a continuous gyration, the originally clear riverbed interface becomes chaotic and disorganized. Here, it might be explained by the Kelvin–Helmholtz (KH) instability phenomenon, the Richardson number (*Ri*) and Froude number (*Fr*).

The Kelvin–Helmholtz instability typically occurs when there is velocity shear in a single continuous fluid, or additionally where there is a velocity difference across the interface between two fluids or the interface between *N* horizontal parallel fluids with different velocities and densities (Lee and Kim, 2015). In this study, the fluid velocity is distributed in a gradient (see Eq. 15), especially where the velocity gradient is relatively large near the riverbed, and the density difference is also large, which is prone to KH instability.

In fact, perturbation is the key factor that induces interface instability and KH instability. In the KH instability, the fluid with high flow velocity in the upper layer will increase the velocity of the low-velocity fluid in the lower layer through viscous action. This makes the interface of different fluid layers forced to perturb. After the fluid crossflow the pipe, a vortex is formed at the tail of the downstream of the pipe, and the magnitude and direction of the velocity change greatly here, and this change increases the perturbations to the interface. And the greater the flow velocity or the greater the pipe exposure, the greater the perturbations.

During the perturbations, the interface between the two fluids is distorted, and a part of the heavy fluid bulges into the upper light fluid. Also, a part of the light fluid will bulge downwards because of the continuity assumption, and the fluids will therefore be mixed. In this process, the heavy fluid protruding upward into the light fluid will not receive enough buoyancy to offset its own weight and will go down again; the same is true for another fluid. In other words, the entire system wants to suppress the occurrence of instability under the action of buoyancy and return to a stable state of "light fluid on top, heavy fluid on bottom". Furthermore, the two parts of the mixed fluid not only exchange positions, but also velocities. The velocity of the denser fluid is increased due to the upper layer drive, while the velocity of the less dense fluid is reduced. For the dense fluid, at the same speed, the Reynolds number increases, and its inertial force also increases (i.e., the fluid is more difficult to be controlled). When it is uncontrollable, the laminar flow turns into turbulent flow, forming a billowing vortex as illustrated in Figures 50, 51, 53 and 54.

For two-dimensional, heterogeneous, unmagnetized flow, a necessary but not sufficient condition for instability is given by the Richardson number:

$$Ri \equiv \frac{g}{\rho}\frac{\partial\rho/\partial z}{\left(\partial u/\partial z\right)^2} < 1/4 \tag{2}$$

is necessary for instability (Lee et al., 2010), where g is gravity (= 9.8 m/s^2), ρ is density, u is a representative flow speed, and z is depth (= Df). It is the dimensionless number that expresses the ratio of the buoyancy term to the flow shear term. If the Richardson number is much less than unity, buoyancy is unimportant in the flow. If it is much greater than unity, buoyancy is dominant (in the sense that there is insufficient kinetic energy to homogenize the fluids).

According to the research in this article, the representative flow speed is the mean velocity (um); the density difference is the difference between the density of the riverbed and the fluid, and the depth is the corresponding D_f. Subsequently, the range of *Ri* number would be 5.8 to 13.36. Obviously, the *Ri* number is much greater than unity, which means that buoyancy is dominant.

Kaminski et al. (2017) have shown that sufficiently large amplitude perturbations with the structure of a linear optimal perturbation can still develop into a 'KH-like' billow state for flows with *Ri* > 1/4, which may perhaps explain why KH billow still occurs when *Ri* is greater than 1/4 in this study. This means that when KH instability occurs, the *Ri* number is not necessarily less than 1/4 (that is, it is not a sufficient condition), and perturbations is the point. It can be seen from Figures 46-54 that KH instability occurs in all cases. The difference is that at higher flow velocity and greater exposed rate, KH billow is more likely to occur (Figures 50, 51, 53 and 54). This shows that the flow velocity and exposed rate have a great influence on the perturbation of the interface.

The Froude number (*Fr*), a dimensionless number, is a cross-sectional flow characteristic defined as $Fr = u/\sqrt{gD}$ (*g* = 9.8 m/s^2). The study of Ramaprabhu et al. (2012) showed that, the terminal *Fr* number of $1/\sqrt{\pi}$ predicted by the classical potential flow theory is achieved and sustained for, but the higher *Fr* number is unstable and may be termed chaotic mixing. The fluid mean velocities selected for this study were 1.8 m/s, 2.2 m/s and 2.6 m/s, corresponding to *Fr* numbers of 0.557, 0.68 and 0.804, respectively. For M5, M6, M8 and M9, the *Fr* number is larger than $1/\sqrt{\pi}$, so the unstable chaos occurs. However, for M2 (Figure 47) and M3 (Figure 48), although their mean fluid velocity has reached 2.2 m/s and 2.6 m/s, the maximum flow velocity around the pipe is only 1.4 m/s and 1.7 m/s because half of the pipe is still buried in the riverbed, and its corresponding *Fr* number is less than $1/\sqrt{\pi}$, so M2 and M3 do not appear to be chaotic.

In addition to the previous factors, the cause of interface chaos may also be related to the contact angle and the surface tension coefficient between the fluid and riverbed because these parameters will affect the direction and magnitude of the shear stress on the riverbed, which leads to some interesting results. Besides, the accumulation of errors in numerical calculations will also lead to instability of the interface. Reducing the calculation error will put higher requirements on the accuracy of the model and computing resources.

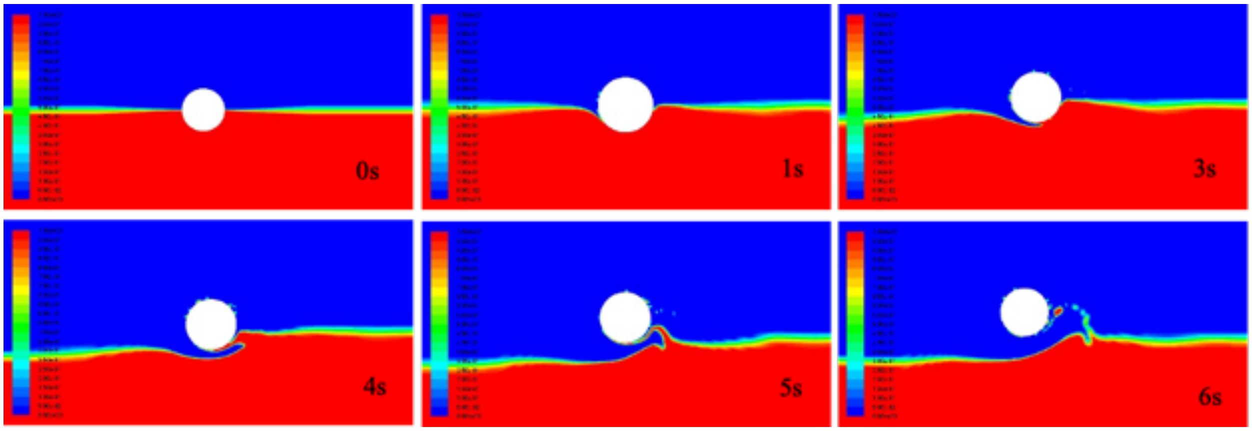

Figure 47. Phase Changes of the Riverbed at Different Moments of Fluid Flow at M1

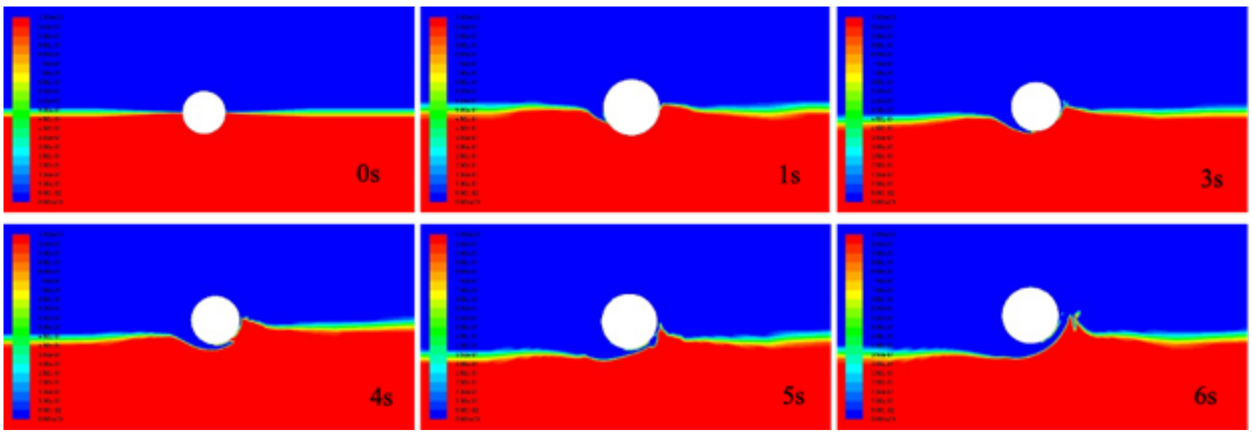

Figure 48. Phase Changes of the Riverbed at Different Moments of Fluid Flow at M2

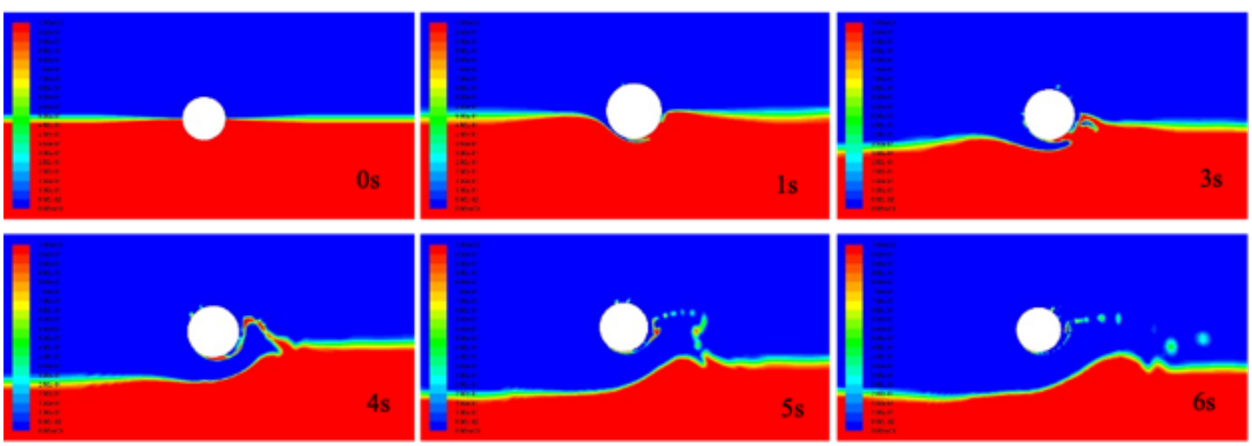

Figure 49. Phase Changes of the Riverbed at Different Moments of Fluid Flow at M3

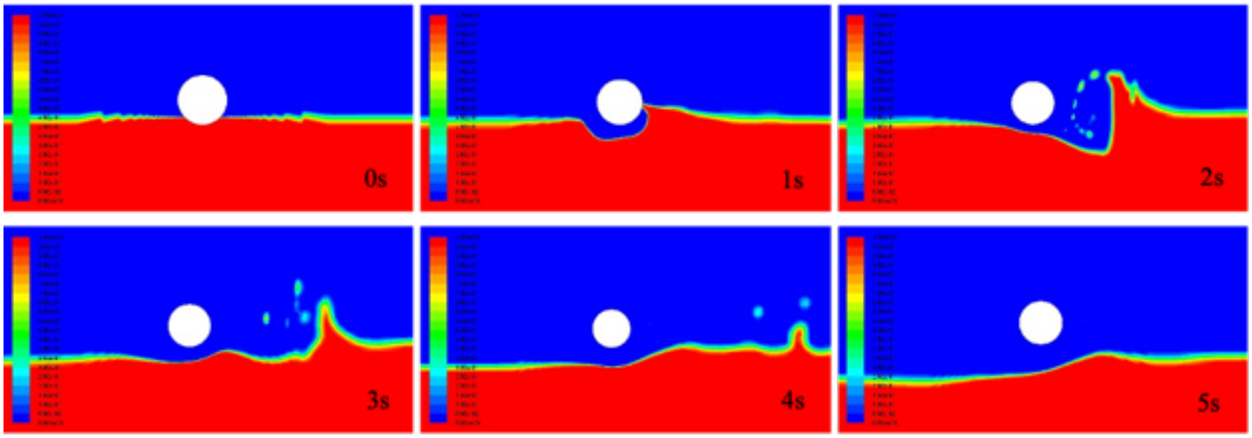

Figure 50. Phase Changes of the Riverbed at Different Moments of Fluid Flow at M4

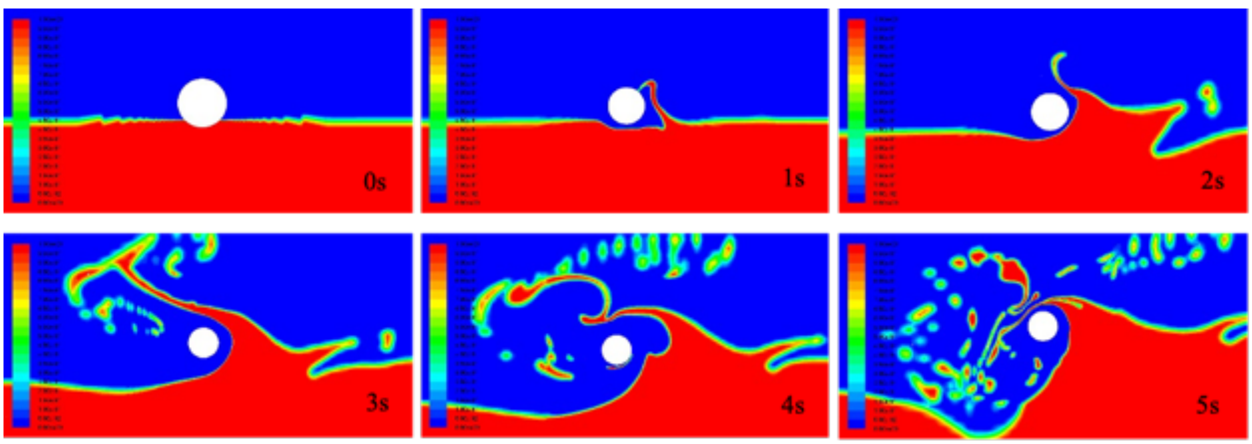

Figure 51. Phase Changes of the Riverbed at Different Moments of Fluid Flow at M5

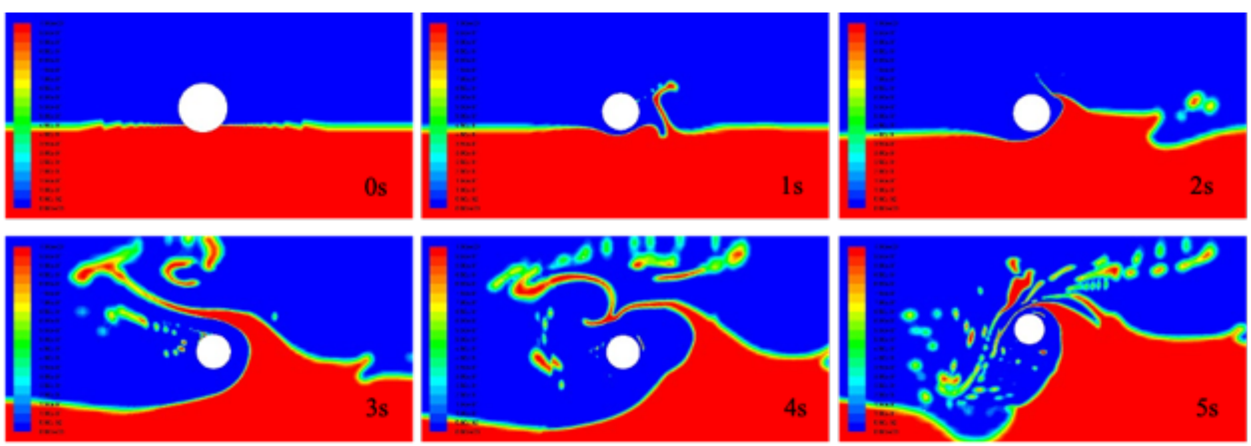

Figure 52. Phase Changes of the Riverbed at Different Moments of Fluid Flow at M6

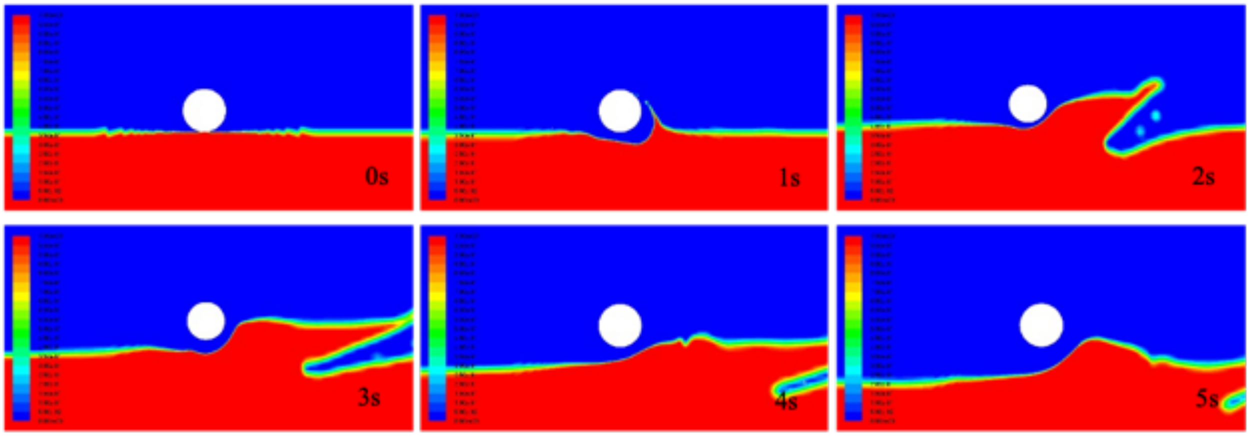

Figure 53. Phase Changes of the Riverbed at Different Moments of Fluid Flow at M7

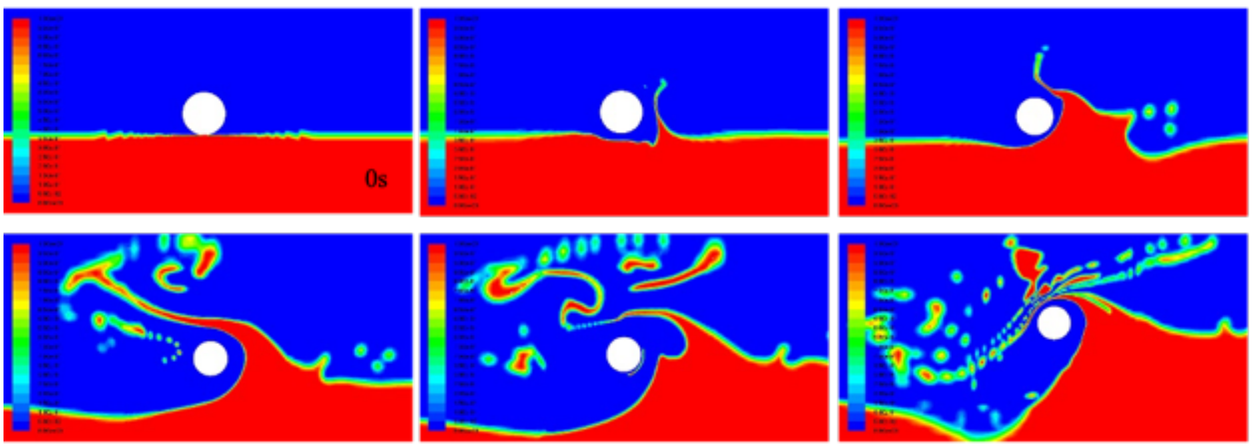

Figure 55. Phase Changes of the Riverbed at Different Moments of Fluid Flow at M8

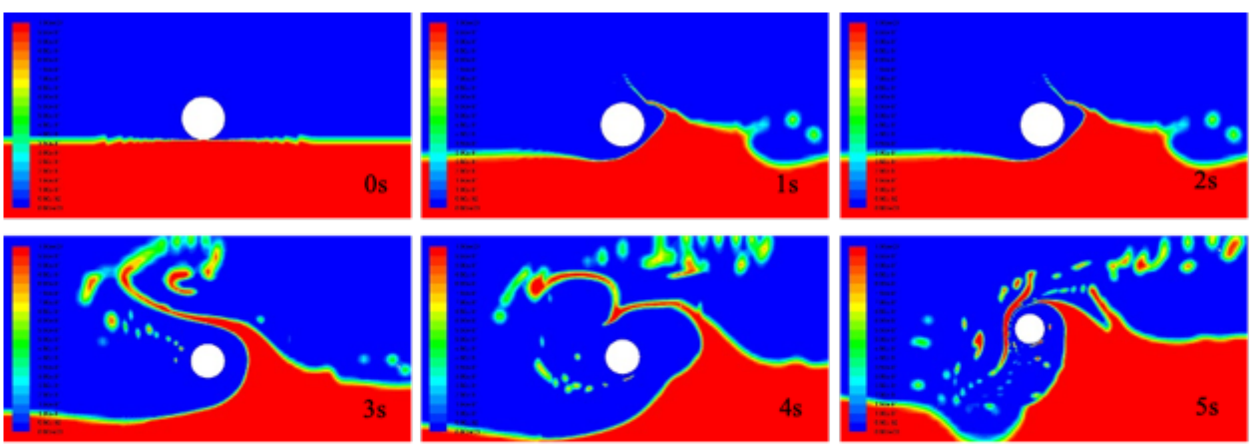

Figure 55. Phase Changes of the Riverbed at Different Moments of Fluid Flow at M9

7.3 Vortex-Induced Vibration Analysis

To clearly understand the Vortex-induced Vibration (VIV) rules of the pipe, the time curves of the fluid forces of each model are listed in Figures 56-58. As seen in the figures, for M1-M4 and M7, the curve is vibrating, especially in the drag direction. But this vibration has no obvious frequency, especially in the lift direction. However, for M5-M6 and M8-M9, this vibration is basically invisible and irregular, and the peak of the fluid force becomes very large. According to the results of the phase diagrams in Section 7.2, it can be known that the riverbed is rolled up in M5-M6 and M8-M9, and the interface is chaotic and disordered, which may cover up the VIV rules, so no obvious VIV can be seen. A Fast Fourier Transformation (FFT) analysis was performed on the fluid force curves of M1-M4 and M7, and it was found that there was no obvious and stable vibration frequency, and there was no "lock-in" phenomenon.

There are two very important parameters that affect VIV, namely Reynolds number R_e and Reduced velocity V_r (Yang et al., 2009). According to the study of Achenbach and Heinecke (1981), qualitative behaviors of fluid flow over a cylinder depends to a large extent on Reynolds number, and similar flow patterns often appear when the shape and Reynolds number is matched. The value of Reynolds number in this study is 1.9×10^6 - 2.8×10^6 (see Table 6), which falls in the turbulent flow regime (i.e., $3\times10^5 < R_e < 3.5\times10^6$). In this flow regime, laminar boundary layer has undergone turbulent transition and wake is narrower and disorganized. Therefore, there is no vortex shedding at the tail of the pipe in this study, and there is no regular vortex vibration.

The physical meaning of V_r number can be explained as the ratio of fluid force acting on the cylinder and the elastic restoring force of the cylinder pipe. For the vortex-induced vibration of the cylinder, V_r number also is an important parameter. According to the study by Yang et al. (2009), when $2< V_r <12$ the amplitude of vibration occurs; When it is approximately 7, the amplitude is largest, where the "lock-in" happens. However, in this study, the maximum V_r number is 0.34 (see Table 6), which is much smaller than the value at the time of vibration. JSME (1998) guideline and ASME (1995) guideline list the bounds for vibration avoidance: When $V_r < 1$, the vibration can be avoided. The V_r number in this study is far from reaching the conditions of vibration. Therefore, none of the research cases in this study have regular VIV, nor will lock-in occur.

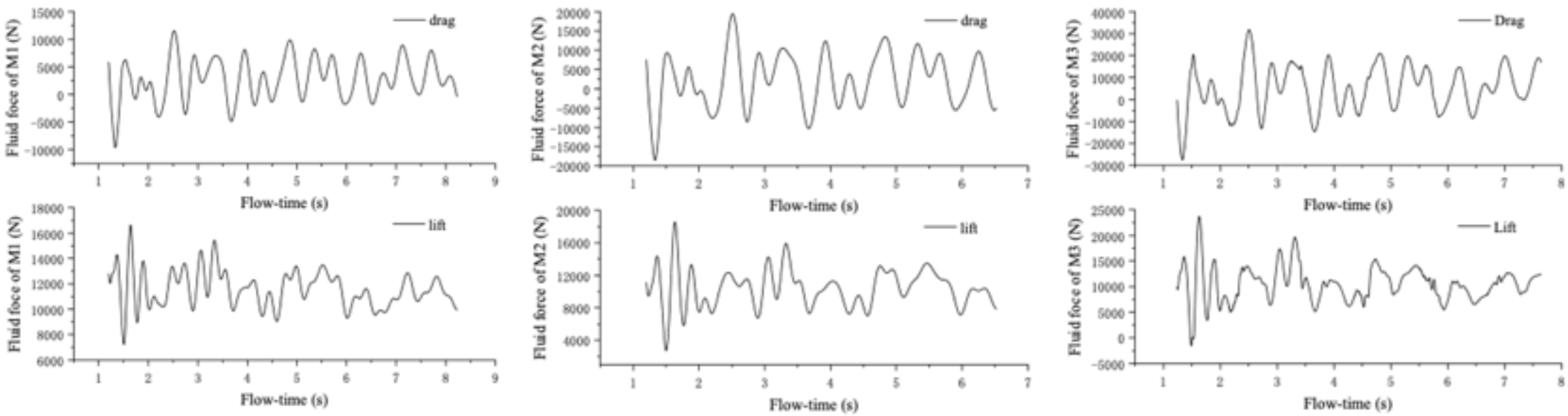

Figure 56. Fluid Force at X Direction (Drag) and Y Direction (Lift) of M1, M2 and M3

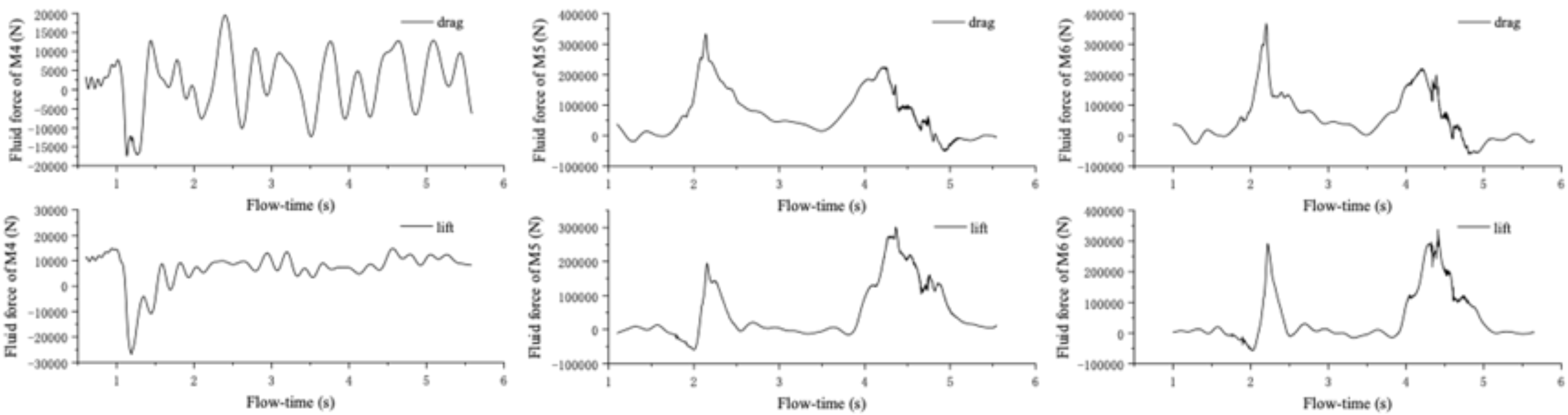

Figure 57. Fluid Force at X Direction (Drag) and Y Direction (Lift) of M4, M5 and M6

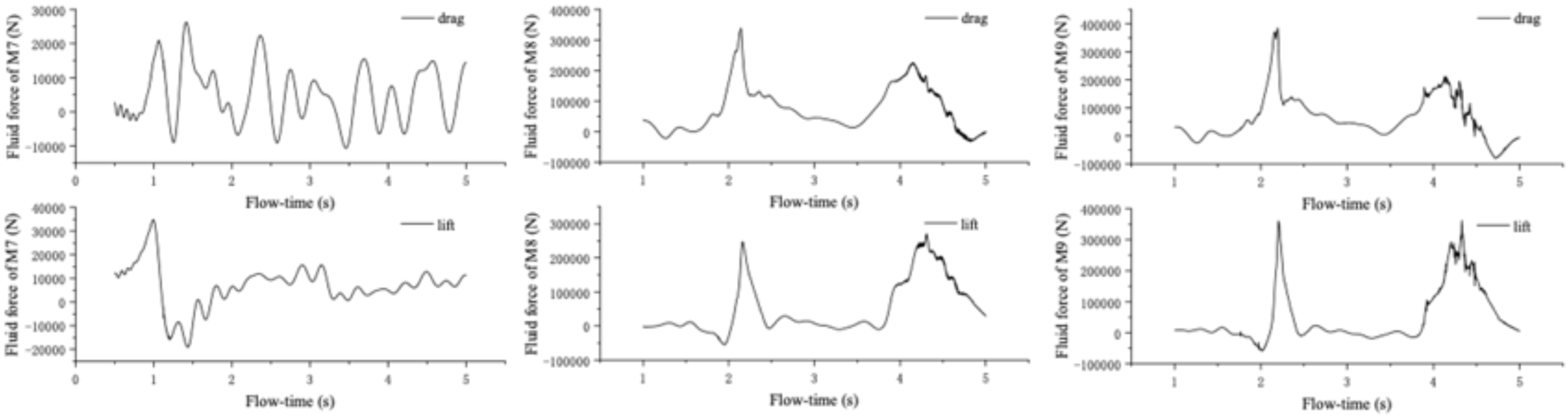

Figure 58. Fluid Force at X Direction (Drag) and Y Direction (Lift) of M7, M8 and M9

7.4 Comparison of Bending Stress of Exposed Pipe caused by Fluid Force

According to the study of Thusyanthan et al. (2014) and McIntosh (2009), the pipeline exposed on the riverbed can be regarded as a structure with two supported ends buried in the riverbed soil and a free span of the exposed part (Figure 59), which can be simplified as a beam structure with simple support at each end supports and subjected to a uniform external force (i.e., fluid force).

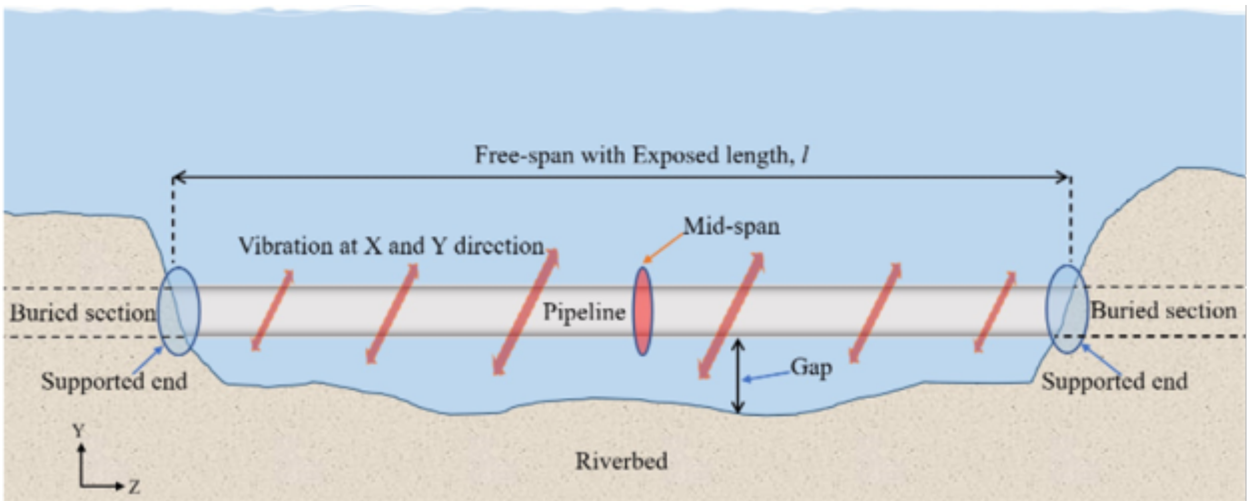

Figure 59. Subsea Pipeline with "Free-span"

Based on the theory of Sun et al. (2002): For the simply supported pipelines with uniformly distributed loads on the surface, the maximum bending normal stress and maximum displacement must occur at the middle position of the free span (mid-span); and the maximum bending shear stress must occur at the position of the support ends. The calculation equations are given below:

Maximum bending normal stress σ_{max} on the pipe caused by external fluid force (x, y axis) is given by,

$$\sigma_{\max} = \frac{M_{\max} y_{\max}}{I_x} \tag{3}$$

Where, y_{max} (= D/2) is the point furthest from the neutral axis; I_x (= I_y) is moment of inertia across the neutral axis.

The maximum bending moment of cross section M_{max} (= $ql^2/8$) is given by,

$$M_{\max} = \frac{ql^2}{8} \tag{4}$$

Where, q is the uniform load acting on the outer surface of the pipe (here it is equal to the lift or drag force in 2D models) and l is the length of pipeline exposed to water. Same as below.

The maximum displacement is given by,

$$\omega_{\max} = \frac{5ql^4}{384EI} \tag{5}$$

Where EI is the bending stiffness of the pipeline.

And the bending shear stress $\tau_{\max}$ on the pipe caused by external fluid force (x, y axis) is given by,

$$\tau_{\max} = 2\frac{F_S}{A} \tag{6}$$

Where, F_S (=ql/2) is the maximum sheer force of cross section; A is the area of the ring section.

Based on the above description, the maximum bending stress and displacement of the pipe, which are at the first peak of the fluid force under the three exposure rates and the three fluid velocities, are extracted and calculated, and are listed in Figures 59-61 and Tables 7-8, respectively. Among them, the lift is the result in the Y direction, and the drag is the result in the X direction, the following are the same.

Figure 59 illustrates that with the increase of fluid velocity and exposure rate, the maximum bending normal stress, shear stress and displacement of the pipeline increase in varying degrees in both X and Y directions. This indicates that the greater the load on the pipeline at higher fluid velocity and greater exposure rate, the more easily it is to be damaged as well. It is noteworthy that when the exposure rate is 75% and 100%, the maximum bending stress of the pipeline under higher fluid velocities (2.2 m/s and 2.6 m/s) has a huge abrupt change compared to that is 50% (see Figures 60-62). The corresponding stress growth multiples are 10.49, 12.30 and 13.33, 15.19 in the Y direction; 17.10, 11.55 and 17.38, 12.11 in the X direction, respectively (see Table 4.3.1). Similarly, compared to the lower fluid velocity of 1.8 m/s, the bending stress of the pipeline also increases significantly at higher velocities (2.2 m/s and 2.6 m/s), and the corresponding stress growth multiples are 7.26, 10.88 and 7.09, 10.32 in the Y direction; 17.06, 18.79 and 12.88, 14.63 in the X direction, respectively. The maximum displacement and shear stress also show the same trend.

Form the analysis, this abrupt change occurs because the riverbed around the pipe is massively rolled up by the incoming flow in these four cases (M5, M6, M8 and M9), which results in a huge and unsteady fluid force deforms the pipe considerably. In these four cases, the maximum bending stress value in the free span of the pipeline is above 3700 MPa, which far exceeds the ultimate tensile strength of 698 MPa of the steel-pipe material, and the maximum displacement value is more than 5 m. Obviously, the pipeline is extremely likely to has been damaged in these four conditions. The next will focus on the other cases M1-M3, M4 and M7.

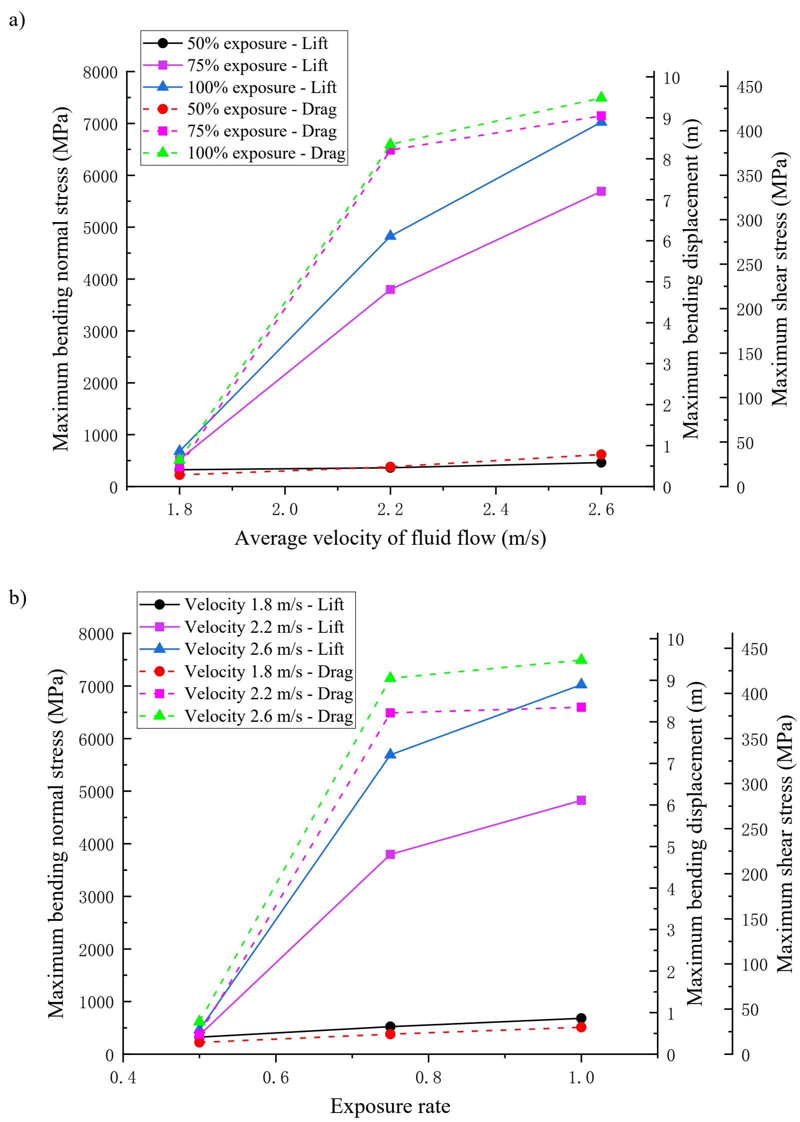

Figure 60. Maximum Bending Normal Stress, Maximum Displacement, and Maximum Shear Stress of the Free Span Pipeline at a) Different Fluid Velocity and b) Different Pipe Exposure Rates with *l* = 36 m

Comparing the results of M1-M3, M4 and M7 (Table 7), as the exposure rate increases, the maximum bending stress of the pipe also increases. Compared to 50% exposure (i.e., M1), the maximum bending stress of the pipe is 2.10 times at Y-direction and 2.28 times at X-direction when it is 100% exposure (i.e., M7); the maximum bending stress of the pipe is 1.61 times at Y-direction and 1.69 times at X-direction when it is 75% exposure (i.e., M4). As seen from the results of M1-M3, the maximum bending stress increases with the increase of fluid velocity at 50% exposure. The maximum bending stress of the pipe at fluid velocities of 2.2 m/s and 2.6 m/s are 1.12 times (Y-direction), 1.69 times (X-direction) and 1.42 times (Y-direction) and 2.75 times (X-direction) of the fluid velocity at 1.8 m/s, respectively. The maximum displacement and the maximum shear stress also show the same trend.

In addition, from the ratio in Table 7, the exposure rate has a greater effect on the mechanics of the pipe in the Y direction; while in the X direction, the fluid velocity has a greater effect. This is because the X direction is consistent with the direction of fluid flow, and the effect of fluid velocity on the pipe is more direct, while in the Y direction, the more exposed to fluid, the more obvious the effect of VIV on the pipe. Whether the increase in the exposure rate or in the fluid velocity, the fluid force and stress on the pipe will increase. This is very detrimental to the oil pipeline exposed on the riverbed.

Then, the maximum bending stress and displacement of the pipe at exposure length l = 18 m were compared and listed in Figures 60-61 and Table 8, respectively. As a result, as the exposed length increases, the bending stress and displacement of the pipe also increase. This trend is inevitable, as evidenced by the formulas of $M_{\max}$, $\omega_{\max}$ and $\tau_{\max}$, and they are power function with the exposure length l (see Table 8). The greater the length of the pipe exposed to fluid, the greater its maximum bending stress and displacement will inevitably increase, and the more easily it is to cause the pipe to destabilization and damage. It can be seen from 7.2 that, as the scouring of the riverbed increases, the length of the pipe exposed to the fluid will gradually increase.

From the above analysis, whether it is an increase of the exposure rate, the fluid velocity, or the length of exposure, the fluid force, the stress, and the displacement on the pipe will increase, which can easily lead the pipe to destabilization and damage. This is very detrimental to the overall oil pipeline. In addition, the exposure rate has a greater effect on the mechanics of the pipe in the lift-direction, while the fluid velocity has a greater effect on the mechanics of the pipe in the drag-direction. Therefore, if the pipe has been exposed, it must take measures immediately for reinforcement and repair. Otherwise, the greater the possibility of pipe bursting, the more losses will be caused.

Table 7. Max Bending Normal Stress, Max Displacement, and Maxi Shear Stress of the Free Span Pipeline with *l* = 36 m

Model No.	$\omega_{max\text{-}Y}$ (m)	$\tau_{max\text{-}Y}$ (MPa)	$\sigma_{max\text{-}Y}$ (MPa)	/M1	/M2	/M3	/M4	/M7	$\omega_{max\text{-}X}$ (m)	$\tau_{max\text{-}X}$ (MPa)	$\sigma_{max\text{-}X}$ (MPa)	/M1	/M2	/M3	/M4	/M7
M1	0.41	18.91	324.37	—	—	—	—	—	0.28	13.10	224.81	—	—	—	—	—
M2	0.46	21.11	362.11	1.12	—	—	—	—	0.48	22.12	379.40	1.69	—	—	—	—
M3	0.58	26.96	462.53	1.42	—	—	—	—	0.78	36.07	618.69	2.75	—	—	—	—
M4	0.66	30.50	523.21	1.61	—	—	—	—	0.48	22.17	380.37	1.69	—	—	—	—
M5	4.81	221.44	3798.7	—	10.49	—	7.26	—	8.21	378.23	6488.3	—	17.10	—	17.06	—
M6	7.20	331.72	5690.5	—	—	12.30	10.88	—	9.04	416.56	7145.8	—	—	11.55	18.79	—
M7	0.86	39.67	680.53	2.10	—	—	—	—	0.65	29.85	512.09	2.28	—	—	—	—
M8	6.11	281.34	4826.2	—	13.33	—	—	7.09	8.35	384.50	6595.9	—	17.38	—	—	12.88
M9	8.89	409.52	7025.1	—	—	15.19	—	10.32	9.48	436.73	7491.8	—	—	12.11	—	14.63

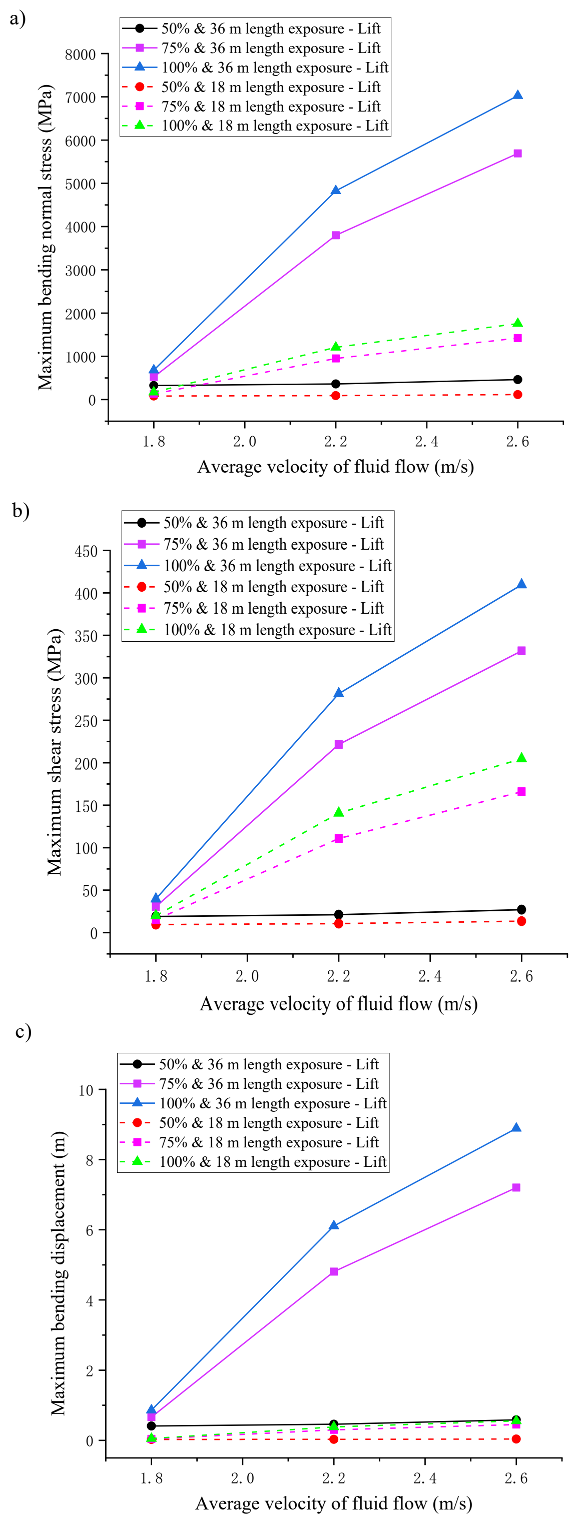

Figure 61. a) Maximum Bending Normal Stress, b) Maximum Shear Stress, and c) Maximum Displacement of the Free Span Pipeline at Y Direction with *l* = 36 m and *l* = 18 m

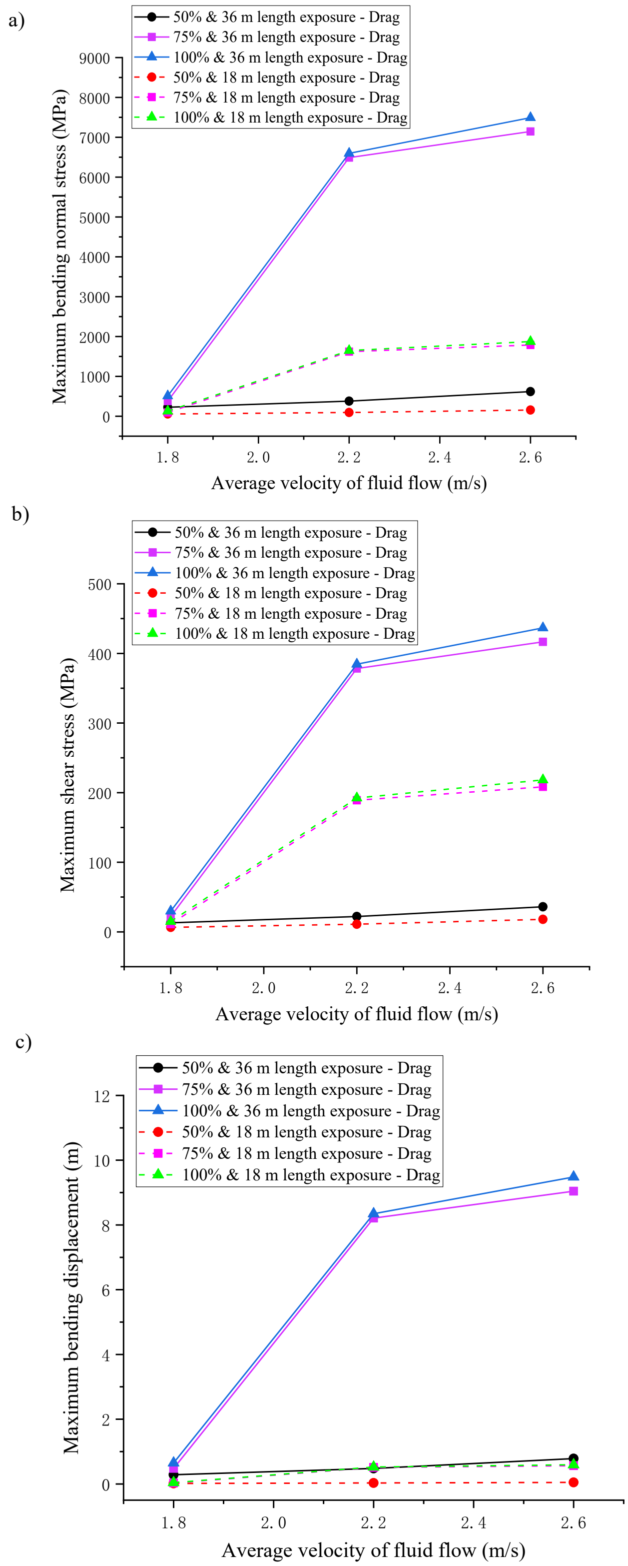

Figure 62. a) Maximum Bending Normal Stress, b) Maximum Shear Stress, and c) Maximum Displacement of the Free Span Pipeline at X Direction with *l* = 36 m and *l* = 18 m

Table 8. Max Bending Normal Stress, Max Displacement and Max Shear Stress of the Free Span Pipeline with *l* = 36 m and *l* = 18 m

Model No.	*l* = 36 m						*l* = 18 m					
	$\omega_{max\text{-}Y}$ (m)	$\sigma_{max\text{-}Y}$ (MPa)	$\tau_{max\text{-}Y}$ (MPa)	$\omega_{max\text{-}X}$ (m)	$\sigma_{max\text{-}X}$ (MPa)	$\tau_{max\text{-}X}$ (MPa)	$\omega_{max\text{-}Y}$ (m)	$\sigma_{max\text{-}Y}$ (MPa)	$\tau_{max\text{-}Y}$ (MPa)	$\omega_{max\text{-}X}$ (m)	$\sigma_{max\text{-}X}$ (MPa)	$\tau_{max\text{-}X}$ (MPa)
M1	0.41	324.37	18.91	0.28	224.81	13.10	0.026	81.09	9.45	0.018	56.20	6.55
M2	0.46	362.11	21.11	0.48	379.40	22.12	0.029	90.53	10.55	0.030	94.85	11.06
M3	0.58	462.53	26.96	0.78	618.69	36.07	0.036	115.63	13.48	0.049	154.67	18.03
M4	0.66	523.21	30.50	0.48	380.37	22.17	0.041	130.80	15.25	0.030	95.09	11.09
M5	4.81	3798.7	221.44	8.21	6488.3	378.23	0.30	949.69	110.72	0.51	1622.08	189.12
M6	7.20	5690.5	331.72	9.04	7145.8	416.56	0.45	1422.63	165.86	0.56	1786.46	208.28
M7	0.86	680.53	39.67	0.65	512.09	29.85	0.054	170.13	19.84	0.041	128.02	14.93
M8	6.11	4826.2	281.34	8.35	6595.9	384.50	0.38	1206.55	140.67	0.52	1648.98	192.25
M9	8.89	7025.1	409.52	9.48	7491.8	436.73	0.56	1756.27	204.76	0.59	1872.96	218.37

7.5 VIV Conclusions

Furthermore, combining the relevant theories of Material Mechanics and the criterion of DNV-RP-F105, the strength and fatigue of the pipeline are analyzed, and the following conclusions are drawn:

- Regardless of the initial exposure rate of the pipeline or the velocity of the fluid, as water flows through the pipeline over an extended period of time, the riverbed soil around the pipeline erodes and disperses eventually resulting in complete exposure. The erosion of the riverbed goes through five stages: onset of scour; tunnel erosion; lee-wake erosion; equilibrium stage; and scour lateral growth. A relatively deep scour pit is formed beneath the pipeline around 6 s, and there is accumulation of riverbed soil near the downstream of the pipe because vortex shedding at the end of the pipe is not obvious enough to cause a higher scour, and the height of the riverbed near the upstream of the pipe has different degrees of reduction caused by scouring. These phenomena are very close to the experimental results of Sumer et al. (1988), Yang et al. (2013) and Gao et al. (2006).

- In this study, the value of Reynolds number is 1.9×10^6 - 2.8×10^6 (see Table 3.4), which falls in the turbulent flow regime (i.e., $3\times10^5 < R_e < 3.5\times10^6$). In this flow regime, laminar boundary layer has undergone turbulent transition and wake is narrower and disorganized. And the maximum V_r number is 0.34 (see Table 3.4), which is much smaller than the value at the time of vibration and far from reaching the conditions of vibration. Therefore, none of the research cases in this paper have regular VIV and vortex shedding at the tail of the pipe, nor will lock-in occur.

- Whether it is an increase of the exposure rate, fluid velocity, or length of exposure, the fluid force, stresses, and displacement on the pipe will increase, which can easily lead the pipeline to destabilization and damage. This is very detrimental to the overall oil pipeline. In addition, the exposure rate has a greater effect on the mechanics of the pipe in the lift-direction, while the fluid velocity has a greater effect on the mechanics of the pipe in the drag-direction.

- As the exposed length of the oil pipeline increases, the influence of external fluid force on its stress increases, and the contribution of internal pressure to its stress decreases. For the free-span submarine pipeline, the external fluid force has a dominant effect on the stress in the free span, and the internal pressure contributes to the stress in its supported ends, and this effect is most obvious at low exposure rates and low flow velocities.

Therefore, if an oil pipeline is exposed to the riverbed, measures must be taken immediately for reinforcement and repair to extend the service life. Failing to act increases the risk of the pipe failing and loss of oil into the waterbody. This will likely result in significant environmental damage to the surround area.

8.0 CONCLUSIONS AND RECOMMENDATIONS

This report presents the development of a River Scour Monitoring Systems (RSS) that provides active monitoring of pipeline crossings to detect the presence of pipe exposure resulting from river scour. The field installation of the River Scour Monitoring Systems (RSS) at five pipelines in three different geographical locations demonstrated the ability to efficiently collect remote data on potential river scour. Location selection for this project was primarily driven by operational partner constraints and shallow cover potential. Data was collected over an 18-month to 19-month period on four pipelines and 4 months on the vandalized unit at the Freeman River. A close temperature alignment was observed between the upstream and downstream RRS units in all installations with the exception of Pipeline #2 of Elk River, which revealed slight deviation between the upstream and downstream RSS units. Bathymetry was collected using a high-resolution multi-beam sonar to create a map of the river channel bottom that revealed no indication that the pipeline was exposed under the water. Depth of cover data was also collected by impressing an AC current on the pipeline and calculating the depth of pipe by measuring the strength of the induced electromagnetic field. The results found that the pipeline was not exposed; however, it was found to have shallow depth of cover in the water channel, which explains the temperature differentials between the upstream and downstream RSS units. The research and field installations indicate that the River Scour Monitoring Systems (RSS) can provide active monitoring for possible river scour, thereby enabling immediate remedial actions to prevent exposure of the buried pipeline. The system is intended to perform similarly on narrow and wide river systems; however, the impact from seasonal flooding is more of an issue and a threat to pipelines in narrower rivers such as those studied in this research.

To reduce the risk of third-party damage to the RSS units, an enhanced perimeter security fencing was placed to provide a deterrent to future potential damage. This physical barrier is necessary as most crossings are in remote areas where the installed RSS units are particularly vulnerable to theft. This was fast-tracked as a result of theft and damage to the RSS unit at the Freeman River Crossing site.

A numerical study was performed on Vortex-Induced Vibration (VIV) of pipelines crossing a river using several scenarios. A Finite Element Model (FEM) was developed to help determine the length of free span that would make a given pipeline susceptible to VIV. Conducting FEM in advance will reduce pipeline damage. In this study, a simulation model of an oil pipeline exposed on a riverbed was created and the volume of fluid (VOF) and user defined functions (UDFs) methods in FLUENT were used to study the influence of the pipeline under the VIV of the fluid.

Future research will be aimed at developing models to predict potential future river scour from collected field data. These models could further help operators in better monitoring and reducing potentially costly pipeline damage and oil spills resulting from river scour. Additionally, continued refinement of the VIV models will enhance our understanding of pipeline failure mechanisms resulting from river scour effects.

9.0 REFERENCES

49 C.F.R. 195. "Transportation of hazardous liquids by pipeline: minimum federal safety standards", 2005

Achenbach, E., Heinecke, E., 1981. "On vortex shedding from smooth and rough cylinders in the range of Reynolds numbers 6×10^3 to 5×10^6." *Journal of Fluid Mechanics*, 109, 239–251. https://doi.org/10.1017/s002211208100102x.

ASME, 1995. Boiler and Pressure Vessel Code Section III, Division I Appendix N, Article N-1300.

Bose J. R., Olson M. K., 1993, "TAPS's leak detection seeks greater precision", *Oil and Gas Journal*, April 5, pp. 43-47.

Carlson B.N., 1993, "Selection and use of pipeline leak detection methods for liability management into the 21st century", *Pipeline Infrastructure II, Proceedings of the International Conference*, ASCE.

de Araújo, J.C., Chaudhry, F.H. 1998. "Experimental Evaluation of 2-D Entropy Model for Open-Channel Flow." *Journal of Hydraulic Engineering*, 124, 1064–1067. https://doi.org/10.1061/(ASCE)0733-9429(1998)124:10(1064).

Fluent Inc., 2006. Fluent 6.3 user's guide. New York, NY, USA.

Gao, F.-P., Yang, B., Wu, Y.X., Yan, S.M., 2006. "Steady current induced seabed scour around a vibrating pipeline." *Applied Ocean Research*, Volume 28, 291–298. https://doi.org/10.1016/j.apor.2007.01.004.

Griebenow G., Mears M., 1988, "Leak detection implementation: modeling and tuning methods", American Society of Mechanical Engineers, Petroleum Division, Vol.19, pp. 9-18

Hough J.E., 1988, "Leak testing of pipelines uses pressure and acoustic velocity", *Oil and Gas Journal*, Vol. 86, No. 47, pp. 35-41.

JSME, 1998. *Guideline for Evaluation of Flow-Induced Vibration of a Cylindrical Structure in a Pipe*. Japanese Society of Mechanical Engineers, Tokyo.

Klein W.R., 1993, "Acoustic leak detection", American Society of Mechanical Engineers, Petroleum Division, Vol. 55, pg. 57-61

Lee, H.G., Kim, J., 2015. "Two-dimensional Kelvin–Helmholtz instabilities of multi-component fluids." *European Journal of Mechanics - B/Fluids,* 49, 77–88. https://doi.org/10.1016/j.euromechflu.2014.08.001.

Liou, J.C.P., Tian J., 1994, "Leak detection: a transient flow simulation approach", American Society of Mechanical Engineers, Petroleum Division, Vol. 60, pp. 51-58

McIntosh, G., 2009. *Risk management in the operations of a subsea pipeline*. IChemE, 5 pp.

Moramarco, T, Saltalippi, C., Singh, V., 2004. Estimation of Mean Velocity in Natural Channels Based on Chiu's Velocity Distribution Equation. Journal of Hydrologic Engineering 9, 42–50. https://doi.org/10.1061/(ASCE)1084-0699(2004)9:1(42).

PHMSA, 2016, "Written statement of the honorable Marie Therese Dominguez, administrator, before the U.S. house of representatives, committee on energy and commerce, subcommittee on energy and power, hearing on examining, pipeline safety reauthorization", *U.S. Department of Transportation*, March 1, Washington, DC.

PHMSA, 2013, "Report to congress: results of hazardous liquid incidents at certain inland water crossings study", United States Department of Transportation, Washington, DC.

Ramaprabhu, P., Dimonte, G., Woodward, P., Fryer, C., Rockefeller, G., Muthuraman, K., Lin, P.-H., Jayaraj, J., 2012. "The late-time dynamics of the single-mode Rayleigh-Taylor instability." *Physics of Fluids*, 24, 74107. https://doi.org/10.1063/1.4733396.

Reuters, 2016, "ExxonMobil to pay $12 million in Montana oil spill settlement", September 21.

Sperl J.L., 1991, "System pinpoints leaks on Point Arguello offshore line", *Oil & Gas Journal,* Sept 9, pp. 47-52

Sumer, M, Ye, M, Fredsøe, J. 1988. "Interaction Between Vibrating Pipe and Erodible Bed." *Journal of Waterway, Port, Coastal, and Ocean Engineering*, ASCE, 114, 81–92

Sun, X., Fang, X., Guan, L. (Eds.), 2002. *Mechanics of Materials (Ⅰ),* 4th ed. Higher Education Press, Beijing, 406 pp.

Thusyanthan, N.I., Sivanesan, K., Murphy, G. (Eds.), 2014. *Free Span Rectification by Pipeline Lowering (PL) Method*. OTC, 10 pp.

Tsahalis, D.T., 1984. “Vortex-Induced Vibrations of a Flexible Cylinder Near a Plane Boundary Exposed to Steady and Wave-Induced Currents.” *Journal of Energy Resources Technology*, 106, 206–213. https://doi.org/10.1115/1.3231039.

Tsahalis, D.T., Jones, W.T. 1981, “Vortex-Induced Vibrations of a Flexible Cylinder Near a Plane Boundary in Steady Flow.” Proceedings of Offshore Technology Conference, Houston, Vol. 3991, pp. 367–386.

Turner N.C., 1991, “Hardware and software techniques for pipeline integrity and leak detection monitoring”, *Proceedings of Offshore Europe*, Vol. 91, Aberdeen, Scotland

Yang, B., Gao, F., Jeng, D.-S., Wu, Y., 2009. “Experimental study of vortex-induced vibrations of a cylinder near a rigid plane boundary in steady flow.” *Acta Mech Sin* 25, 51–63. https://doi.org/10.1007/s10409-008-0221-7.

Yang, B., Yang, T., Ma, J.-L., Cui, J.-S., 2013. “The experimental study on local scour around a circular pipe undergoing vortex-induced vibration in steady flow.” *Journal of Marine Science and Technology*, 21, 250–257. https://doi.org/10.6119/JMST-012-0412-2.

APPENDIX A – Samples of Daily Data Collected

Samples of Daily Data Collected (every 10 minutes)

Table 1. Tongue River Pipeline #1 Sample Data

	Upstream 1 (V)	Upstream 1 (°C)	Upstream 1 (°C)	Upstream 1 (°C)	Upstream 2 (V)	Upstream 2 (°C)	Upstream 2 (°C)	Upstream 2 (°C)	Downstream (V)	Downstream (°C)	Downstream (°C)	Downstream (°C)
	Battery (Internal)	Channel 0 - Silicon (Ground)	Channel 1 - Internal	Channel 1 - Silicon (Pipe)	Battery (Internal)	Channel 0 - Silicon (Ground)	Channel 1 - Internal (Disconnected)	Channel 1 - Silicon (Pipe)	Battery (Internal)	Channel 0 - Silicon (Ground)	Channel 1 - Internal (Disconnected)	Channel 1 - Silicon (Pipe)
Date		Position: 0 (m)	Position: 0 (m)	Position: 0 (m)	Position: 89.5014	Position: 89.501472 (m)	Position: 89.501472 (m)	Position: 89.501472 (m)	Position: 915.899	Position: 915.899616 (m)	Position: 915.899616 (m)	Position: 915.899616 (m)
2020-3-20 07:02	13.70770428	4.938476226	-13.96888457	5.005000854	12.80057679	2.829328833	-14.57685658	4.989159862	13.30453651	2.067955431	-15.81212274	5.008954727
2020-3-20 07:12	13.70770428	4.938346511	-14.08342816	5.00367736	12.80057679	2.829902081	-14.95684633	4.988506934	13.30453651	2.067313778	-15.65565946	5.008245799
2020-3-20 07:22	13.70770428	4.937980837	-14.17086166	5.003216842	12.80057679	2.831615761	-15.06201006	4.989473909	13.30453651	2.066471471	-15.82442328	5.007886967
2020-3-20 07:32	13.70770428	4.938048385	-14.36385184	5.003408476	12.80057679	2.829986061	-15.098762	4.988453979	13.30453651	2.066580729	-15.80453992	5.007859328
2020-3-20 07:42	13.70770428	4.938310137	-14.65983434	5.004394295	12.80057679	2.833091678	-15.26488561	4.990595725	13.30453651	2.067561719	-16.01286367	5.008519102
2020-3-20 07:52	13.70770428	4.938249861	-14.76754409	5.005356291	12.80057679	2.833629273	-15.56912424	4.99232125	13.30453651	2.069292546	-16.42720877	5.009255821
2020-3-20 08:02	13.70770428	4.938175648	-15.06723283	5.005904897	12.80057679	2.832191015	-15.87574138	4.992017412	13.30453651	2.069224926	-16.76550417	5.009994316

Table 2. Tongue River Pipeline #2 Sample Data

	Upstream 1 (V)	Upstream 1 (°C)	Upstream 1 (°C)	Upstream 1 (°C)	Upstream 2 (V)	Upstream 2 (°C)	Upstream 2 (°C)	Upstream 2 (°C)	Downstream (V)	Downstream (°C)	Downstream (°C)	Downstream (°C)
	Battery (Internal)	Channel 0 - Silicon (Ground)	Channel 1 - Internal (Internal)	Channel 1 - Silicon (Pipe)	Battery (Internal)	Channel 0 - Silicon (Ground)	Channel 1 - Internal (Internal)	Channel 1 - Silicon (Pipe)	Battery (Internal)	Channel 0 - Silicon (Ground)	Channel 1 - Internal (Internal)	Channel 1 - Silicon (Pipe)
Date	Position: 0 (m)	Position: 0 (m)	Position: 0 (m)	Position: 0 (m)	Position: 1266.89	Position: 1266.89 (m)	Position: 1266.89 (m)	Position: 1266.89 (m)	Position: 1354.29 (m)	Position: 1354.29 (m)	Position: 1354.29 (m)	Position: 1354.29 (m)
2020-3-20 07:09	11.8934493	7.876928363	-13.02553963	10.45293359	13.70770428	3.438161904	-15.82946062	10.38681144	13.40532845	5.426793047	-15.70018639	10.46298138
2020-3-20 07:19	11.8934493	7.876098118	-13.19479203	10.45337163	13.70770428	3.437937289	-16.1483457	10.38652923	13.40532845	5.428681407	-15.87754185	10.46446289
2020-3-20 07:29	11.8934493	7.87609899	-13.35908074	10.45510941	13.70770428	3.43824508	-15.95159988	10.38759192	13.40532845	5.426776306	-15.61534469	10.4644498
2020-3-20 07:39	11.8934493	7.875766071	-13.71887291	10.45564462	13.70770428	3.437557822	-16.07730948	10.38864491	13.40532845	5.426923019	-15.78258256	10.46535997
2020-3-20 07:49	11.8934493	7.875402442	-13.95733718	10.46352393	13.70770428	3.438094128	-16.17444004	10.39666291	13.40532845	5.426966259	-16.03423113	10.47252359
2020-3-20 07:59	11.8934493	7.874795266	-14.50549785	10.45978106	13.70770428	3.438600421	-16.45672138	10.39238555	13.40532845	5.428650763	-16.42729179	10.4709533
2020-3-20 08:09	11.8934493	7.87483223	-14.16939367	10.46104305	13.70770428	3.438761652	-16.91856863	10.39360637	13.40532845	5.424535988	-17.12008225	10.46726507

Table 3. Elk River Pipeline #1 Sample Data

	Upstream 1 (V)	Upstream 1 (°C)	Upstream 1 (°C)	Upstream 1 (°C)	Upstream 2 (V)	Upstream 2 (°C)	Upstream 2 (°C)	Upstream 2 (°C)	Downstream (V)	Downstream (°C)	Downstream (°C)	Downstream (°C)
	Battery (Internal)	Channel 0 - Silicon (Ground)	Channel 1 - Internal (Disconnected)	Channel 1 - Silicon (Pipe)	Battery (Internal)	Channel 0 - Silicon (Ground)	Channel 1 - Internal (Disconnected)	Channel 1 - Silicon (Pipe)	Battery (Internal)	Channel 0 - Silicon (Ground)	Channel 1 - Internal (Disconnected)	Channel 1 - Silicon (Pipe)
Date	Position: 0.3048 (	Position: 0.3048 (m)	Position: 0.3048 (m)	Position: 0.3048 (m)	Position: 804.38 (	Position: 804.38 (m)	Position: 804.38 (m)	Position: 804.38 (m)	Position: 1042.38	Position: 1042.38 (m)	Position: 1042.38 (m)	Position: 1042.38 (m)
2020-3-20 07:08	13.30453651	13.88428554	7.388894966	13.7477427	12.09503319	12.14451354	6.971548683	13.37456662	11.8934493	12.74947792	8.430711453	13.30141748
2020-3-20 07:18	13.30453651	13.88847073	7.234365056	13.7417341	12.09503319	12.1458819	6.878080532	13.36798685	11.8934493	12.74590679	8.25657956	13.29396484
2020-3-20 07:28	13.30453651	13.89276292	7.172229407	13.73536384	12.09503319	12.14726429	6.78840448	13.36180522	11.8934493	12.7423997	8.211014382	13.28720878
2020-3-20 07:38	13.30453651	13.89724313	7.03115653	13.72986719	12.09503319	12.14869332	6.592713106	13.35538388	11.8934493	12.73877316	8.212740758	13.28020414
2020-3-20 07:48	13.30453651	13.9015997	6.778698949	13.7286141	12.09503319	12.15015131	6.47619	13.35140307	11.8934493	12.73539674	8.033157704	13.27504733
2020-3-20 07:58	13.30453651	13.9054654	6.629497109	13.72415619	12.09503319	12.15150488	6.154038942	13.34655678	11.8934493	12.73186366	7.868459387	13.26976681
2020-3-20 08:08	13.30453651	13.90905282	6.670385985	13.70552314	12.09503319	12.15278819	6.051095368	13.33792152	11.8934493	12.7284925	7.603958127	13.26162676

Table 4. Elk River Pipeline #2 Sample Data

	Upstream 1 (V)	Upstream 1 (°C)	Upstream 1 (°C)	Upstream 1 (°C)	Upstream 2 (V)	Upstream 2 (°C)	Upstream 2 (°C)	Upstream 2 (°C)	Downstream (V)	Downstream (°C)	Downstream (°C)	Downstream (°C)
	Battery (Internal)	Channel 0 - Silicon (Ground)	Channel 1 - Internal (Disconnected)	Channel 1 - Silicon (Pipe)	Battery (Internal)	Channel 0 - Silicon (Ground)	Channel 1 - Internal (Disconnected)	Channel 1 - Silicon (Pipe)	Battery (Internal)	Channel 0 - Silicon (Ground)	Channel 1 - Internal (Disconnected)	Channel 1 - Silicon (Pipe)
Date	Position: 0 (m)	Position: 0 (m)	Position: 0 (m)	Position: 0 (m)	Position: 802.92 (	Position: 802.92 (m)	Position: 802.92 (m)	Position: 802.92 (m)	Position: 1711.58	Position: 1711.58 (m)	Position: 1711.58 (m)	Position: 1711.58 (m)
2020-3-20 07:09	13.00216068	15.73921021	7.36162478	18.9841414	13.20374456	18.72437625	6.724131634	19.04682601	13.20374456	18.69087761	9.050482615	18.02303883
2020-3-20 07:19	13.00216068	15.73886529	7.385812091	18.98218351	13.20374456	18.71905552	6.42993383	19.04701053	13.20374456	18.69065366	9.02983	18.02503999
2020-3-20 07:29	13.00216068	15.73847178	7.148268554	18.98009537	13.20374456	18.71019293	6.103527687	19.03873616	13.20374456	18.68264496	9.010173112	18.01952877
2020-3-20 07:39	13.00216068	15.73853836	7.06263647	18.97783941	13.20374456	18.70207451	5.97333563	19.03662539	13.20374456	18.68239494	8.831630655	18.02209755
2020-3-20 07:49	13.00216068	15.7388639	7.030992388	18.97621274	13.20374456	18.69382616	5.918667284	19.03538311	13.20374456	18.67865528	8.318981945	18.0190712
2020-3-20 07:59	13.00216068	15.73884668	6.937086286	18.97454744	13.20374456	18.68505622	5.594297064	19.03322747	13.20374456	18.67696832	8.310438193	18.01796457
2020-3-20 08:09	13.00216068	15.73900408	6.778774624	18.97141887	13.20374456	18.67358062	5.423196241	19.0314546	13.20374456	18.67978775	8.293498755	18.02034439

Table 5. Freeman River Pipeline #1 Sample Data

	Upstream 1 (V)	Upstream 1 (°C)	Upstream 1 (°C)	Upstream 1 (°C)	Upstream 2 (V)	Upstream 2 (°C)	Upstream 2 (°C)	Upstream 2 (°C)	Downstream (V)	Downstream (°C)	Downstream (°C)	Downstream (°C)
	Battery (Internal)	Channel 0 - Silicon (Groun	Channel 1 - Internal (Discon	Channel 1 - Silicon (Pipe)	Battery (Internal)	Channel 0 - Silicon (Ground)	Channel 1 - Internal (Disco	Channel 1 - Silicon (Pipe)	Battery (Internal)	Channel 0 - Silicon (Ground)	Channel 1 - Internal (Disconnected)	Channel 1 - Silicon (Pipe)
Date	Position: 0.01 (m)	Position: 0.01 (m)	Position: 0.01 (m)	Position: 0.01 (m)	Position: 446.56 (m)	Position: 446.56 (m)	Position: 446.56 (m)	Position: 446.56 (m)	Position: 946.22 (n	Position: 946.22 (m)	Position: 946.22 (m)	Position: 946.22 (m)
2020-7-7 05:06	13.80849622	11.18585803	10.6665748	11.06661895	13.70770428	7.237619522	9.861942285	10.24336885	12.80057679	10.94504531	11.33048886	10.80595083
2020-7-7 05:16	13.80849622	11.18592153	11.01394375	11.06540939	13.70770428	7.238376048	10.06956749	10.24244696	12.80057679	10.94520068	11.32224636	10.80476592
2020-7-7 05:26	13.80849622	11.18611591	11.11856906	11.06417216	13.70770428	7.23901522	10.07224766	10.24069632	12.80057679	10.94538244	11.02451937	10.80425664
2020-7-7 05:36	13.80849622	11.18648461	11.18840738	11.06263403	13.70770428	7.24003708	10.08840058	10.23879579	12.80057679	10.94585006	11.02682284	10.8034351
2020-7-7 05:46	13.80849622	11.18672104	11.28564816	11.06117809	13.70770428	7.241203079	10.45013485	10.23661334	12.80057679	10.94617704	11.12518467	10.80305415
2020-7-7 05:56	13.80849622	11.18687462	11.49239565	11.05982498	13.70770428	7.242279833	10.6075133	10.23497455	12.80057679	10.94607423	11.1934013	10.80212664